Spectroscopy for E and S0 galaxies in nine clusters

Inger Jørgensen,[1,2,4]★ Marijn Franx[3,4]★ and Per Kjærgaard[1]★

[1] *Copenhagen University Observatory, Øster Voldgade 3, DK-1350 Copenhagen, Denmark*
[2] *McDonald Observatory, The University of Texas at Austin, RLM 15.308, Austin, TX 78712, USA (Postal address for IJ)*
[3] *Kapteyn Institute, PO Box 800, 9700 A V Groningen, The Netherlands (Postal address for MF)*
[4] *Center for Astrophysics, 60 Garden Street, Cambridge, MA 02138, USA*

ABSTRACT

Central velocity dispersions, Mg_2 line indices and radial velocities for 220 E and S0 galaxies are derived on the basis of intermediate resolution spectroscopy. Galaxies in the following clusters have been observed: Abell 194, Abell 539, Abell 3381, Abell 3574, S639, S753, Doradus, HydraI (Abell 1060) and Grm 15. For 151 of the galaxies, the velocity dispersion has not previously been measured. 134 of the Mg_2 determinations are for galaxies with no previous measurement. The spectra cover either 500 or 1000 Å, centred on the magnesium triplet at 5177 Å. The observations were obtained with the Boller & Chivens spectrograph at the ESO 1.5-m telescope and with OPTOPUS, a multi-object fibre-fed B&C spectrograph, at the ESO 3.6-m telescope. The data are part of our ongoing study of the large-scale motions in the Universe and the physical background for the Fundamental Plane.

The Fourier fitting method was used to derive the velocity dispersions and radial velocities. The velocity dispersions have been corrected for the effect of the size of the aperture. The correction was established on the basis of velocity dispersion profiles available in the literature. A comparison with results from Davies et al. shows that the derived central velocity dispersions have an rms error of 0.036 in $\log \sigma$. There is no offset relative to the velocity dispersions from Davies et al. The offset relative to data from Lucey & Carter is -0.017 ± 0.011 in $\log \sigma$, with our velocity dispersions being the smallest. The velocity dispersions derived from the B&C and the OPTOPUS observations, as well as the velocity dispersions published by Davies et al., Dressler, Lucey & Carter and Lucey et al., can be brought on a system consistent within 3 per cent.

The Mg_2 line indices have been corrected for the size of the apertures, transformed to the Lick system, and corrected for the effect of the velocity dispersion. From comparison with data from Davies et al. and from Faber, we find that the rms error of Mg_2 is 0.013. Comparisons of the radial velocities with data from the literature show that our determinations are accurate to within ≈ 35 km s^{-1}. The accuracies reached for these observations are adequate for the study of the large-scale motions in the Universe and for investigations of the Fundamental Plane.

Key words: techniques: spectroscopic – galaxies: clusters: general – galaxies: elliptical and lenticular, cD – galaxies: fundamental parameters.

1 INTRODUCTION

The D_n–σ relation was introduced as a distance determinator for E galaxies by Dressler et al. (1987b). Dressler and collaborators were the first to apply the method to a large sample of galaxies. Their data showed the presence of a large-scale motion, which they interpreted as being due to a huge mass concentration, the so-called 'Great Attractor' (Dressler et al. 1987a; Lynden-Bell et al. 1988).

The interpretation of the data is, however, still uncertain. Mathewson, Ford & Buchhorn (1992) did not detect the expected backside infall towards the 'Great Attractor', and recently Courteau et al. (1993) found evidence for a bulk

★ E-mail addresses: inger@ydun.as.utexas.edu; franx@cosmos.astro.rug.nl; per@astro.ku.dk

flow that includes all galaxies out to a radial velocity of 6000 km s^{-1}. We have therefore undertaken an observing programme to provide independent measurements of distances and peculiar velocities for E and S0 galaxies. We also use our data for a thorough study of the methods, the D_n–σ relation, as well as of the Fundamental Plane (FP), $\log r_e = a \log \sigma + b \langle \mu \rangle_e + c$ (Djorgovski & Davis 1987). The first results from our investigation show that the D_n–σ relation can be regarded as an approximation to the FP, and that the FP is likely to give more accurate distances to the galaxies (Jørgensen, Franx & Kjærgaard 1993; see also Phillips 1988). Also, Lucey et al. (1991) found a very low scatter for the FP for the Coma cluster.

The accurate determination of central velocity dispersions is important for the use of the FP and the D_n–σ relation: a 5 per cent uncertainty in the velocity dispersion relates into a similar uncertainty in the distance determination. Several methods have been developed for deriving velocity dispersions (see, e.g., Rix & White 1992, and references therein). We use the Fourier fitting method (Franx, Illingworth & Heckman 1989a) which, like the Fourier Quotient method (Sargent et al. 1977), assumes the broadening function to be Gaussian. The determination of the uncertainty is, however, more straightforward in the Fourier fitting method.

In this paper we present the spectroscopic data, which constitute the main body of the velocity dispersions and Mg$_2$ indices used in our study of the FP and the large-scale motions in the Universe. Central velocity dispersions, Mg$_2$ indices and radial velocities for galaxies in nine clusters are derived: Abell 194, Abell 539, Abell 3381, Abell 3574, S639, S753 and HydraI (Abell 1060), from Abell, Corwin, Jr & Olowin (1989), and Doradus and Grm 15, from Maia, da Costa & Latham (1989). Photometry for the galaxies is presented in Jørgensen, Franx & Kjærgaard (1995a) and Jørgensen (1993). The FP for the clusters is analysed in Jørgensen, Franx & Kjærgaard (1995b).

The paper is organized as follows. Sample selection and observations are described in Section 2, the basic reduction of the spectra is covered in Section 3, and the central velocity dispersions, the Mg$_2$ indices and the radial velocities are derived in Section 4. The effects of noise in the spectra are discussed in Section 5, where we also establish and apply aperture corrections. In Section 6 the results are compared internally and with results from the literature. Section 7 summarizes these results. The individual measurements of the parameters are listed in the Appendix. Table 4 gives the aperture-corrected mean values of the velocity dispersions and the Mg$_2$ line indices, consistent with the data from Davies et al. (1987), as well as the radial velocities.

2   SAMPLES AND OBSERVATIONS

The original intention was to observe the 176 E and S0 galaxies in nine galaxy clusters for which we have obtained CCD photometry (see Jørgensen et al. 1995a). We have observed 131 of these galaxies. The five brightest members of each cluster were observed. The rest of the spectroscopic sample was chosen randomly among our photometric sample. 54 additional galaxies in A539, A3381, S639 and HydraI were observed in order to make full use of the available fibres during our observations with the fibre-fed spectrograph OPTOPUS (see below). The main selection

criteria for these 54 galaxies were type and total magnitude. Further, 26 galaxies in other clusters or in the field have been observed for comparison purposes. The sample also includes nine galaxies in Hickson compact groups (Hickson 1982). In total, 220 galaxies were observed.

The observations were carried out during three observing runs at the ESO 1.5-m telescope, equipped with the Boller & Chivens spectrograph (hereafter B&C), and one observing run at the ESO 3.6-m telescope with the OPTOPUS instrument. OPTOPUS is a fibre-fed B&C spectrograph which enables multiple object spectroscopy of 50 objects within the field of 33 arcmin. Normally, five to seven fibres are used for sky spectra. OPTOPUS is described in Cristiani et al. (1987).

Dates, instrumentation, wavelength range and spectral resolution are summarized in Table 1. The exposure time and the position angle of the slit for the observations with the B&C spectrograph are given in the Appendix. We were aiming at a signal-to-noise ratio (S/N) of 25 per Å for the galaxies and higher than 100 per Å for the template stars.

Five fields in the four clusters A539, A3381, S639 and HydraI were observed with OPTOPUS. The positions and identifications for the galaxies are given in the Appendix. The positions were measured on ESO/SRC sky survey plates with the OPTRONIC plate measuring machine at ESO, Garching. A comparison of the derived positions of galaxies in A539 and A3381 with the positions listed by Dressler (1980) shows an overall rms scatter of 1–2 arcsec. The positions of the galaxies in HydraI have been compared with the positions given by Lucey & Carter (1988); here the rms scatter is 0.6 arcsec. All OPTOPUS fields were observed twice, each observation having an exposure time of 1 h.

K giant stars were observed to serve as template stars in the determination of the velocity dispersion. Some of these are also radial velocity standard stars. A few spectrophotometric standard stars were observed. As many of the observations were carried out under non-photometric conditions, only a relative flux calibration was possible.

Table 2 lists the observed K giants and spectrophotometric standard stars. During the observations of the K giants, the 1.5-m telescope was moved slightly, in order to get the signal to fill the slit in a similar way as for an extended object. Two different techniques were used for the observation of stars with OPTOPUS: either the telescope was slightly defocused and the signal recorded in four to six fibres, or it was focused and the signal was recorded in one fibre. The last technique proved to be the most useful, as it led to the highest S/N in the spectra.

3   BASIC REDUCTION OF THE SPECTRA

3.1   Boller & Chivens spectra

The steps used in the reduction of the B&C spectra were as follows:

(i) subtraction of bias, dark current and scattered light;
(ii) flat-field correction for pixel-to-pixel variations;
(iii) removal of signal from cosmic-ray events;
(iv) wavelength calibration and geometric rectification;
(v) subtraction of the sky background;
(vi) determination of the velocity dispersion and the radial velocity (cf. Section 4.1);

Table 1. Instrumentation for the observing runs.

	B&C-1	B&C-2	B&C-3	OPTOPUS
Dates	Oct. 8–13, 1990	April 13–17, 1991	Jan. 25–28, 1992	Feb. 1–2, 1992
Telescope	ESO 1.5m	ESO 1.5m	ESO 1.5m	ESO 3.6m
Instrument	B&C	B&C	B&C	OPTOPUS
Grating	#10 2nd order	#10 2nd order	#10 2nd order	#19 2nd order
Dispersion	67Å/mm	67Å/mm	67Å/mm	59Å/mm
Wavelength range	4700–5700Å	4700–5700Å	4265–6260Å[a]	5000–5620Å
Slit	2.5 arcsec	2.5 arcsec	2.5 arcsec	2.6 arcsec[b]
Instrumental dispersion (σ)[c]	1.24Å, 72km/s	1.24Å, 72km/s	1.32Å, 77km/s	1.17Å, 68km/s
CCD	RCA ESO #13	RCA ESO #13	FA ESO #27	Tek ESO #16
Read-out-noise	64e⁻	69e⁻	10.5e⁻	9.2e⁻
Conversion factor	2.6e⁻/ADU	4e⁻/ADU	2.7e⁻/ADU	2.8e⁻/ADU
Spatial scale	2.72 arcsec/pix[d]	2.72 arcsec/pix[d]	1.36 arcsec/pix[e]	–
Slit length	2′.77	2′.77	2′.77	–
Number of E and S0 galaxies	57	31	32	113

The velocity dispersions are derived from the wavelength interval 4700–5550 Å (B&C) or 5000–5550 Å (OPTOPUS).

[a] The wavelength range is limited by vignetting, the useful wavelength range is 4450–6160 Å.

[b] Diameter of optical fibre.

[c] The instrumental dispersion is determined as sigma in a Gaussian fit to lines in calibration spectra and to sky emission lines. The equivalent dispersion in km s^{-1} is determined at 5177 Å.

[d] CCD binned four times in spatial direction.

[e] CCD binned two times in spatial direction.

Table 2. K giants and spectrophotometric standard stars.

Star	Observing runs
K giants:	
HD6055	B&C-1
HD28191	B&C-3
HD28322	OPTOPUS
HD77236	B&C-1, B&C-2, B&C-3
HD116292	OPTOPUS
HD120223*	B&C-2, B&C-3, OPTOPUS
HD123123	OPTOPUS
HD172401	B&C-2
HD176047*	B&C-1, B&C-2
HD196983*	B&C-1, B&C-2
HD207241	B&C-1
BD −43°2527*	B&C-1, B&C-3
Spectrophotometric standard stars:	
Feige 67	B&C-3
Feige 110	B&C-1
40 Eri B	B&C-1, B&C-3
Hiltner600	B&C-2, B&C-3
HD117880	OPTOPUS
L 870-2	B&C-1
LTT7379	B&C-2

The stars marked * are radial velocity standards.

(vii) flux calibration to give the relative flux; and

(viii) determination of the Mg$_2$ line index (cf. Section 4.2).

These steps are described in detail below.

The image processing system IRAF[1] was used for the basic reduction. Subtraction of bias and dark current was carried out using median-filtered mean frames calculated from many single exposures. The scattered light was determined from 25 or 50 columns at about 60 arcsec from the end of the slit. A low-order polynomial was fitted to these columns and the fit was subtracted from the spectrum.

Correction for the variation of the pixel-to-pixel sensitivity was carried out with dome flat-fields, each one being a mean of 10 single flat-fields. The flat-fields were normalized by fitting a polynomial to the continuum in the wavelength direction and dividing the flat-field by the fit. A comparison of different flat-fields showed low-frequency variations of less than 0.5 per cent. The pixel-to-pixel noise in the resulting flat-fields, due to the photon noise, was 0.2 per cent in the red end of the spectrum and 0.5 per cent in the blue end.

Observations of the twilight sky indicated that no correction for the slit profile was necessary. The variations along the slit are less than 0.3 per cent except for 30 arcsec in the east end of the slit (with the slit in east–west direction). Even at the east end the variations are below 1 per cent.

Pixels that contained signal from cosmic-ray events were located by first modelling the profile of the galaxy in the spatial direction. The model was then scaled to the local spectrum row and subtracted. Pixels that deviated by more than seven times the local standard deviation in the residual image were identified as cosmic-ray events. All other pixels were set to zero. This resulted in a mask image, which was subtracted from the original image. The technique worked well for images without emission lines and with relatively low background level. Areas with strong night sky emission lines had to be flagged, and signal from cosmic-ray events could not be removed in these areas. Cosmic-ray events fainter than seven times the standard deviation are still present in the spectra, but were found not to affect the determination of the spectroscopic parameters.

The wavelength calibration of the spectra was derived using Helium–Argon lamp spectra (HeAr). High signal-to-noise HeAr images were determined as the mean of 10–20 single exposures obtained in the day-time. In the night-time,

---

[1] IRAF is distributed by National Optical Astronomy Observatories, which is operated by the Association of Universities for Research in Astronomy, Inc., under cooperative agreement with the National Science Foundation, USA.

HeAr exposures were obtained every second hour. A comparison of the high signal-to-noise HeAr images with the night-time exposures showed typical wavelength differences of ± 0.25 pixel (≈ 0.25 Å, equivalent to an uncertainty on the derived radial velocities of 15 km s^{-1}). This is more than sufficient for the accuracy of the wavelength calibration that we are aiming at. The final wavelength calibration was therefore carried out using the high signal-to-noise HeAr images with no extra offset of the science spectra.

The spectra of the galaxies were rectified on the basis of both the HeAr images and the spectra themselves (to correct for the S-distortion). The spectra were binned logarithmically in wavelength. The sky background was subtracted, and the sky spectrum was kept in the first row of the spectra to make it possible to calculate the signal-to-noise ratio.

3.1 OPTOPUS spectra

The steps in the reduction of the OPTOPUS spectra were as follows:

(i) subtraction of bias, dark current and scattered light;
(ii) flat-field correction for pixel-to-pixel variations;
(iii) extraction of the spectra with simultaneous removal of signal from cosmic-ray events, wavelength calibration, normalization to the mean fibre throughput, and subtraction of sky background (the IRAF script task DOFIBERS was used for this step);
(iv) determination of the velocity dispersion and the radial velocity (cf. Section 4.1);
(v) flux calibration to give the relative flux; and
(vi) determination of the Mg$_2$ line index (cf. Section 4.2).

The OPTOPUS spectra were corrected for bias and dark current in the same way as the B&C spectra. Each spectrum in an OPTOPUS observation has a width of 4 pixel, and the spectra are separated by 2 pixel. The scattered light was determined by fitting a cubic spline to the pixel values in the areas of the detector where no signal from the fibre was present. Each dimension was fitted independently and the correction image was smoothed before subtraction to avoid introducing low-frequency noise in the image.

Correction for the pixel-to-pixel variations in the detector sensitivity was carried out with a two-dimensional mean flat-field determined from 10 lamp flat-fields. The flat-field was normalized by fitting the continuum in the wavelength direction with a cubic spline and dividing the flat-field by the fit. Pixels with count levels below 400 ADU were set to one in the normalized flat-field, and no flat-field correction was made for these pixels. This ensured that no spurious effects were introduced at the low signal edges of the spectra, and that the noise in the normalized flat-field was below 1 per cent.

We used the IRAF script task DOFIBERS for the extraction of the spectra. The extraction was carried out with variance weighting over the spectral profile and simultaneous removal of signal from cosmic-ray events. Wavelength calibration, normalization to the mean fibre throughput, and subtraction of the sky background are also included in DOFIBERS.

The response dependence on the wavelength changed slightly for each set-up. Dome flat-fields taken in the night-time were used to correct for this effect. The resulting spectra have a flat continuum.

The wavelength calibration of the spectra was derived using Helium–Neon lamp spectra (HeNe). High signal-to-noise HeNe images were determined as the mean of 10–20 single exposures obtained in the day-time. In the night-time, HeNe exposures were obtained in connection with each 1-h exposure. These were used to determine the offsets relative to the day-time HeNe images. The offsets were in general less than 0.15 Å. The final wavelength calibration was checked from the position of the sky line at 5577 Å. The centre of the line had an rms scatter of 0.22 Å and a min/max variation of ± 0.6 Å. The rms scatter is equivalent to an uncertainty on the derived radial velocities of 13 km s^{-1}. The spectra were binned logarithmically in wavelength.

The relative throughput of the fibres changes with each set-up and was therefore derived for each spectrum. This was done using a first extraction of the spectra, where the sky background was not subtracted. The night sky emission line at 5577 Å was fitted with a Gaussian and the total flux was used as a measurement of the relative fibre throughput. The extraction was then re-done with normalization to the mean fibre throughput, and the sky background was subtracted. The sky spectrum was the average sky spectrum recorded with five to seven fibres. The determination of the relative throughput of the fibres was iterated two to three times from the residuals of the 5577-Å sky line. The residuals from this strong line after the final sky subtraction are mainly due to the uncertainty in the wavelength calibration. The total flux in the residuals was less than 3 per cent of the flux before subtraction. For 80 per cent of the galaxies, the intensity of the sky, excluding the flux from the 5577-Å line, was less than 30 per cent of the intensity of the galaxy. Thus, for 80 per cent of the galaxies, the possible residual intensity from the sky is less than 1 per cent of the intensity of the galaxy.

The signal from some strong cosmic-ray events was not properly removed by the cleaning option during the extraction. Pixels affected by these cosmic-ray events were located by comparison of the extracted spectra from the two observations of the same field. In this process, the spectra were scaled to each other and the difference computed. Pixels in the difference images that deviated more than five times the local standard deviation were identified as cosmic-ray events. A mask image for each spectrum was determined by setting all other pixels in the difference image to zero. The mask image was then subtracted. The net effect of this was to substitute the pixels that contained signal from cosmic-ray events with the pixel values from the other observation, properly scaled. The drawback for the method is that the interpolation during the extraction of the spectra smeared the cosmic-ray events somewhat. However, since only very strong signal from cosmic-ray events passes the cleaning in IRAF, typically if a cosmic-ray event covers all four pixels in the spectral profile of a fibre, the remaining cosmic-ray events can be unambiguously identified even from the extracted spectra.

4 DETERMINATION OF SPECTROSCOPIC PARAMETERS

The velocity dispersions and the radial velocities were derived from the non-flux-calibrated spectra, which were binned logarithmically in wavelength. The Mg$_2$ indices were

derived after the relative flux calibration and from spectra binned linearly in wavelength.

4.1 Velocity dispersion and radial velocity

Several methods for determining the velocity dispersions and radial velocities for galaxies have been introduced over the last 10–15 yr (see Rix & White 1992, and references therein). We apply the Fourier fitting method as described in Franx et al. (1989a; see also van der Marel & Franx 1993). The broadening function is assumed to be Gaussian. It is not possible to obtain more detailed information about the shape of the line profiles from our spectra because of the limited S/N ratios. See Rix & White (1992) for a discussion of how to analyse the line profiles in the case of asymmetric profiles.

The parameters in the broadening function were determined by minimizing

$$\chi^2 = \sum_{k=k_l}^{k_h} |\tilde{G}(k) - \tilde{B}(k)\tilde{S}(k)|^2. \tag{1}$$

$\tilde{G}(k)$, $\tilde{S}(k)$ and $\tilde{B}(k)$ are the Fourier transforms of the galaxy spectrum, the spectrum of the template star, and the broadening function, respectively. χ^2 is determined in the Fourier space in order to gain computational speed.

The method was implemented in a program created by MF. The program reads images in IRAF format. When the sky spectrum is present in the image, the signal-to-noise for the spectrum can be calculated. The output is in the form of ASCII files that contain the derived parameters and their uncertainties, plus an IRAF image of the extracted galaxy spectrum, the normalized and continuum-subtracted galaxy spectrum, the Fourier power spectrum for the galaxy, the galaxy spectrum with the low and high frequencies filtered out, and the same information for the template star. In addition, the cross-correlation and the residuum for the fit are given.

The program fits a low-order polynomial (fifth order) to the continuum of both the galaxy and the star. The continuum is subtracted and a cosine bell is used to fix the end points to zero. The Fourier transforms are calculated and the high and low frequencies (user-defined limits) are filtered out. We used lower limits of $k_l = 5$ or 10 $[\approx (100 \text{ Å})^{-1}]$ and higher limits of $k_h = 256$ or 512 $[\approx (2 \text{ Å})^{-1}]$ for spectra with wavelength ranges of 500 and 1000 Å respectively. The lower limit is applied with a cosine bell, and is thus effectively a soft cut-off.

For the B&C spectra, the mean spectra over 8.16 arcsec (B&C-1 and B&C-2) or 6.8 arcsec (B&C-3) in the spatial direction were fitted. The signal-to-noise ratio and the spatial resolution in the spectra were not sufficient to derive radial profiles for the parameters.

For the OPTOPUS spectra, the fitting was carried out on the extracted spectra, which covers an aperture with a diameter of 2.6 arcsec. In order to retain the original counting statistics, the OPTOPUS spectra were scaled to the original mean count level. This scaled spectrum, together with a scaled sky spectrum, was used as the input for the Fourier fitting program. If one of the two OPTOPUS spectra for a given galaxy had S/N < 20, the Fourier fitting was done using the weighted mean spectrum instead of the two spectra individually. This limits the possible systematic effects intro-

duced by low S/N (cf. Section 5). We compared parameters derived from mean spectra with the mean parameters from the individual spectra. For spectra with S/N ≥ 20 this comparison showed no systematic effects and the rms scatter of log σ was 0.005.

Template stars of spectral type G8–K3 result in significantly better fits than stars of types K4–K5. The K4–K5 stars were therefore not used for the final determinations. Table 2 lists the template stars used. The rms scatter of the differences between the determinations with different template stars was typically ±0.010 on log σ and ±2 km s^{-1} on the radial velocity. All differences were within the formal uncertainties on the parameters. The possible systematic effects arising from the choice of template stars are discussed further in Section 6.1.2. The velocity dispersions and radial velocities were derived as the mean of the results from the different template stars. The radial velocities were corrected for the radial velocity of the template star and corrected to the heliocentric system. The result is given as cz_{hel}.

4.2 The Mg$_2$ line index

The Mg$_2$ line indices were derived from the flux-calibrated spectra. The Lick definition of the line and continuum bands for the index was used (Worthey et al. 1994). For some of the galaxies observed with OPTOPUS, the Mg$_2$ index has not been derived because part of the continuum bands was outside the wavelength range. Low-S/N OPTOPUS spectra were averaged before the determination of the Mg$_2$ index.

In order to ensure the best possible consistency with the Lick system, we first convolved our spectra to the Lick/IDS instrumental dispersion of 200 km s^{-1} (González 1993). The spectra were then binned linearly in wavelength, flux-calibrated, and the Mg$_2$ indices were derived. For the B&C observations, the indices were derived from the mean spectra of the central 8.16 arcsec (B&C-1 and B&C-2) or 6.8 arcsec (B&C-3).

5 RESULTS AND APPLIED CORRECTIONS

The individual measurements of the spectroscopic parameters are tabulated in the Appendix. In the following, we discuss the effects of noise, the correction for the size of the apertures, and the correction of Mg$_2$ for the effect of the velocity dispersion. The internal consistency and comparison with published results are covered in Section 6.

The individual measurements of the velocity dispersions and the Mg$_2$ line indices have been aperture-corrected to a circular aperture with metric diameter of 1.19 h^{-1} kpc ($H_0 = 100$ h^{-1} km s^{-1} Mpc^{-1}), equivalent to 3.4 arcsec at the distance of the Coma cluster (cf. Section 5.2). There is an offset between the velocity dispersions derived from the B&C spectra and those from the OPTOPUS spectra. We have added 0.024 to the value of log σ derived from the OPTOPUS spectra in order to make these measurements consistent with the velocity dispersions derived from the B&C spectra (cf. Section 6.1).

Variance-weighted mean values of log σ, Mg$_2$ and cz_{hel} have been derived for all the galaxies observed. The Mg$_2$ indices were offset so as to be consistent with the Lick system (Section 6.2) and corrected to zero velocity dispersion (Section 5.3). The mean values of the parameters are

tabulated in Table 4. We also list $\log \sigma$ and Mg_2 aperture-corrected to a circular aperture with diameter $r_e/4$, where r_e is the effective radius of the galaxy. The uncertainties of the velocity dispersions are the formal uncertainties as derived in the Fourier fitting method. The uncertainties on Mg_2 are the internal uncertainties based on the S/N ratio of the spectra. The internal uncertainty of the radial velocity is dominated by the uncertainty in the wavelength calibration, and is typically 17 km s^{-1}. Velocity dispersions were derived for 220 galaxies; 151 of these have no previous measurements. The Mg_2 line index was derived for 173 galaxies; 134 of these are new measurements.

In Table 5 we list velocity dispersions and Mg_2 indices from the literature for galaxies in Abell 194, DC 2345−28 and the Coma cluster with our aperture corrections applied. These literature data are used in the analysis of the FP (Jørgensen et al. 1995b), together with our own data. The offsets applied to make the literature data consistent with Davies et al. (1987) are given in the table. The uncertainties of these offsets are typically 0.01 in $\log \sigma$ and 0.003 in Mg_2.

5.1   The effects of the noise

The formal uncertainty on the velocity disperson is dependent on the S/N in the spectrum, the galaxy velocity dispersion compared with the instrumental dispersion, and to a lesser extent on the wavelength interval used for the determination. Figs 1 and 2 show the formal relative uncertainty as a function of the S/N per Å and as a function of the velocity dispersion. The smallest formal uncertainty that can be reached with our instrumental dispersion (and template stars) is $\simeq 4$ per cent. For B&C observations with S/N ≥ 25 and OPTOPUS observations with S/N ≥ 30, the formal uncertainty is below 6 per cent and the external error sources are expected to dominate. The uncertainty on the velocity dispersion depends approximately on the S/N as

$$\frac{\Delta \sigma}{\sigma} \simeq \frac{1.4}{S/N} \qquad \text{for B\&S spectra,}$$

and

$$\frac{\Delta \sigma}{\sigma} \simeq \frac{1.8}{S/N} \qquad \text{for OCTOPUS spectra.}$$

These relations are overplotted in Figs 1 and 2. We tested the effect of the shorter wavelength range for the OPTOPUS spectra by fitting the B&C spectra with the wavelength range limited to that of the OPTOPUS spectra. This resulted in
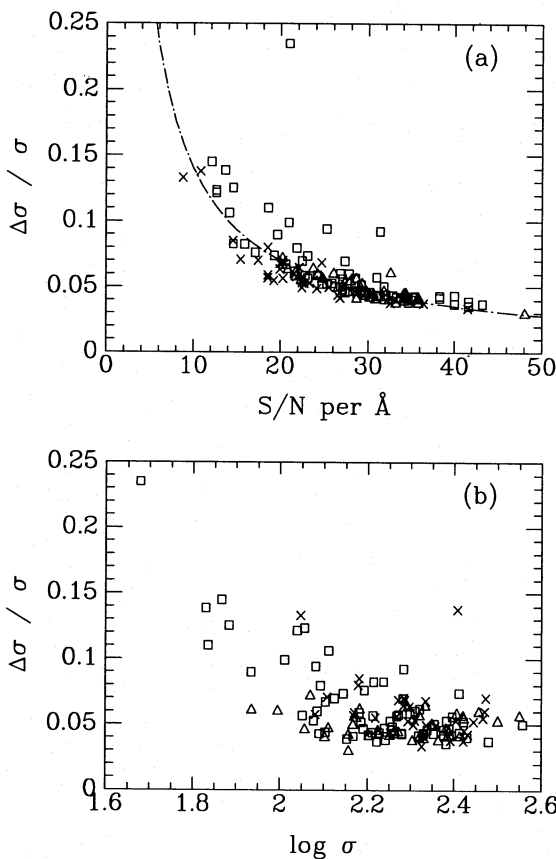
Figure 1. The relative formal uncertainty on the velocity dispersion as a function of (a) the S/N per Å for the spectrum, and (b) the velocity dispersion. Boxes – B&C-1; triangles – B&C-2; crosses – B&C-3. To reach a formal uncertainty of 6 per cent, a S/N of 25 per Å is required.
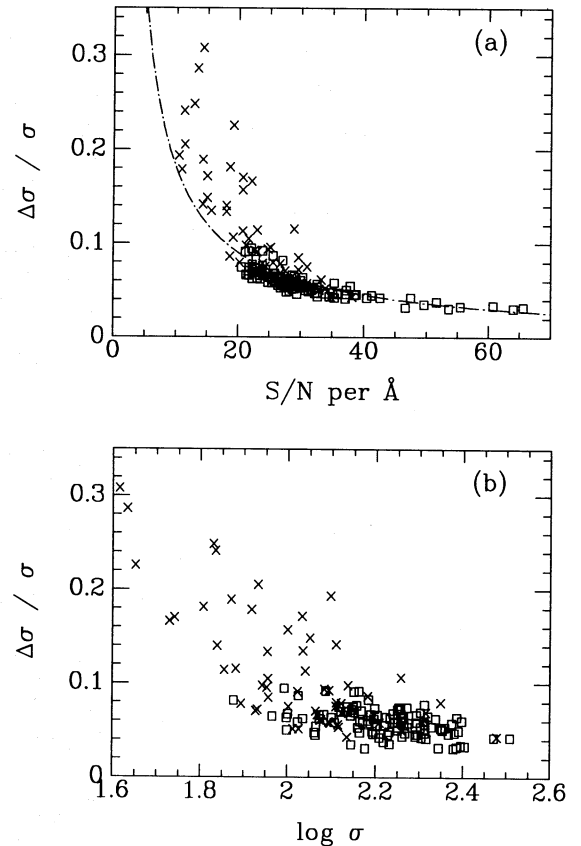
Figure 2. The relative formal uncertainty on the individual velocity dispersions derived from OPTOPUS spectra, as a function of (a) the S/N per Å, and (b) the velocity dispersion. Boxes – determinations from individual spectra with S/N ≥ 20; crosses – determinations from mean spectra. To reach a formal uncertainty of 6 per cent, a S/N of 30 per Å is required.

$\Delta\sigma/\sigma \approx 1.7/(\text{S/N})$. Thus, much of the higher uncertainty on the OPTOPUS data at a given S/N is due to the smaller wavelength range. The uncertainty on the radial velocity relative to the velocity dispersion depends on the S/N of the spectrum in a similar way; $\Delta v/\sigma$ is smaller than $\Delta\sigma/\sigma$ by about a factor of 1.5.

The formal relative uncertainty on the velocity dispersion rises for $\log\sigma \lesssim 2.0$. Although most of the galaxies with low velocity dispersion are also those with low S/N, a few of the galaxies with $\log\sigma \lesssim 2.0$ have larger uncertainties than expected from the S/N.

We have investigated further the effects of noise in the spectra from simulations. A high S/N spectrum of a template star observed with OPTOPUS was convolved with Gaussians with σ spanning velocity dispersions from 65 to 300 km s^{-1}. Noise was added to give S/N ratios of 10, 15, 20, 30 and 40. The velocity dispersion and radial velocity were then derived with the original high S/N spectrum of the star as the template. Variance-weighted mean values of $\log\sigma$ and the radial velocity were determined from 1000 simulations of each combination of velocity dispersion and S/N. The simulations show the same dependence of the formal relative uncertainties on the S/N as the data, and the simulations with a velocity dispersion of 65 km s^{-1} have the highest relative uncertainties.

Fig. 3 shows the relative systematic errors of the derived mean velocity dispersions. At low S/N, the mean velocity dispersion is systematically too large, except for $\sigma = 300$ km s^{-1}. The low-velocity-dispersion galaxies are subject to the largest systematic effects. The systematic effect is less than 1 per cent for simulations with S/N ≥ 15 and $\sigma \geq 100$ km s^{-1}. For these simulations, the systematic effect is approximately a factor of 10 smaller than the formal uncertainty at a given S/N. For low-velocity-dispersion galaxies, the velocity dispersion derived from low S/N spectra may be subject to systematic errors of 0.02–0.04 in $\log\sigma$.

5.2 Aperture corrections

E and S0 galaxies have radial gradients in the radial velocity, velocity dispersion and the Mg$_2$ line index. Therefore, the derived 'central' parameters depend on the distances of the galaxies and the size of the aperture used for the observation. We apply an aperture correction to correct the observed parameters to a system that is independent of distance and telescope. Davies et al. (1987) established an aperture correction based on nearby galaxies observed through small apertures $(4 \times 4 \text{ arcsec}^2)$ and through large apertures $(16 \times 16 \text{ arcsec}^2)$. They used a very simple interpolation function for their correction.
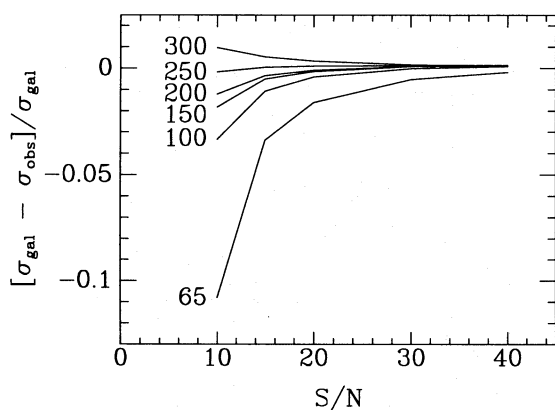
We have established an aperture correction from kinematic models based on data available in the literature. Published galaxy photometry and kinematics were used to construct two-dimensional models of the surface brightness, velocity dispersion and rotational velocity projected on the sky. These models are obtained by interpolation of the photometry, and kinematics, and are therefore entirely empirical. Kinematic data were taken from Davies et al. (1983), Davies & Birkinshaw (1988), Franx et al. (1989a), Jedrzejewski & Schechter (1989), van der Marel, Binney & Davies (1990) and Fisher, Illingworth & Franx (1995). The surface photometry was taken from Djorgovski (1985), Jedrzejewski (1987), Bender, Döbereiner & Möllenhoff (1988), Franx, Illingworth & Heckman (1989b) and Peletier et al. (1990). The necessary data were available for 51 galaxies. The velocity dispersion measured through an aperture is equal to the luminosity-weighted second moment of the velocity distribution. This also includes a contribution due to rotation. The empirical models were used to determine how the observed velocity dispersion depends on various aperture shapes and sizes.

First, we investigated the effect of the position angle difference between a rectangular aperture and the major axis of the observed galaxy. For typical rectangular apertures of our observations, the mean variation is within ± 0.5 per cent in the velocity dispersion for position angle differences between zero and 90°. The rms scatter is of the same size. We therefore decided not to take this effect into account.

We used the models to derive the equivalent circular apertures for each of our rectangular apertures. The models predict that dispersions observed through both apertures have the same mean value. The dimensions of the rectangular apertures and the equivalent diameters, $2r_{ap}$, of the circular apertures are given in Table 3. Note that, for these aperture sizes, $2r_{ap} \approx 1.025 \times 2(xy/\pi)^{1/2}$ within ± 4 per cent, where x and y are the width and the length of the rectangular aperture.

We then used the models to calculate how the observed velocity dispersion depends on (circular) aperture size. The

Figure 3. The relative systematic errors on the velocity dispersion as a function of the S/N per Å, as derived from simulations. The curves are labelled with the input velocity dispersion in km s^{-1}.

Table 3. Apertures.

Data source		Slit	Fiber diameter	$2r_{ap}$
B&C-1, B&C-2		2″5 × 8″16		5″00
B&C-3		2″5 × 6″8		4″70
OPTOPUS			2″6	2″60
Davies et al. (1987)	LICK	1″5 × 4″0		2″95
Davies et al. (1987)	LCOLO	2″0 × 4″0		3″28
Davies et al. (1987)	LCOHI	4″0 × 4″0		4″56
Davies et al. (1987)	KPNO	2″3 × 4″2		3″57
Davies et al. (1987)	AAT	2″0 × 7″0		4″50
Lucey & Carter (1988)			2″7	2″70
Lucey et al. (1991)		2″0 × 5″8		3″90

model values were normalized to σ_{e8}, which is the dispersion measured through an aperture with a radius of $r_e/8$. Fig. 4(a) shows the median values of these normalized synthetic measurements as a function of the size of the apertures. Inside an effective radius, the profile is well described by a power law,

$$\frac{\sigma_{ap}}{\sigma_{e8}} = \left(\frac{r_{ap}}{r_e/8}\right)^{-0.04}. \tag{2}$$

The power law approximates the curve to within 1 per cent for $r < r_e/2$. This is sufficiently accurate for most purposes. If a higher accuracy is needed, a second-order fit produces

$$\log\frac{\sigma_{ap}}{\sigma_e} = -0.065 \log\left(\frac{r_{ap}}{r_e}\right) - 0.013\left[\log\left(\frac{r_{ap}}{r_e}\right)\right]^2, \tag{3}$$

where σ_e is the dispersion measured through an aperture with radius r_e.

We have also determined power-law coefficients for individual galaxies. The power-law slopes correlate weakly with velocity dispersion and ellipticity of the galaxy. Galaxies with low velocity dispersions or high ellipticity have slightly shallower profiles. The systematic variation is about 0.02 over the full range, compared with an FWHM scatter in the power-law slope of 0.06. The inclusion of the weak trends does not reduce the scatter significantly, and we have ignored these trends.

Fig. 4(b) shows the distribution of the ratio of aperture radius to effective radius for the galaxies in our programme. The spread is fairly large, because the galaxies span a wide range in effective radius. We have normalized the dispersions

to an aperture radius of $r_e/8$. As an alternative, we can correct the velocity dispersion to an aperture with a standard physical size. This is particularly easy, as we have shown above that the correction is well approximated by a power law. Therefore, this correction is completely independent of the effective radius. Fig. 4(c) shows the median values of the synthetic velocity dispersion measurements as a function of the physical radius of the aperture. The measurements were normalized to an aperture with diameter $2r_{norm} = 1.19 \ h^{-1}$ kpc. Again, the power law provides a good fit:

$$\log\frac{\sigma_{ap}}{\sigma_{norm}} = -0.04 \log\frac{r_{ap}}{r_{norm}}. \tag{4}$$

The normalization diameter is equivalent to 3.4 arcsec projected on to a galaxy in Coma. The aperture correction adopted by Davies et al. (1987) is also shown in Fig. 4(c). It approximates the curve reasonably well for $r < 2r_{norm}$. Fig. 4(d) shows the distribution of r_{ap}/r_{norm} for our data. The distribution is quite narrow. The corrections are therefore generally smaller than when the velocity dispersions are normalized to an aperture with radius $r_e/8$.

The relative distances for the galaxies were derived from the cluster radial velocities in the CMB system. The values are given in Jørgensen et al. (1995a). For the 26 comparison galaxies, the radial velocities were taken from Faber et al. (1989).

Davies, Sadler & Peletier (1993) found the mean of the radial gradients in Mg_2 for E galaxies to be -0.059. Thus, the Mg_2 gradients are similar to the radial gradients in $\log\sigma$ (cf. Franx et al. 1989a). We have therefore adopted the same aperture correction for Mg_2 as for $\log\sigma$, i.e. Mg_2 was
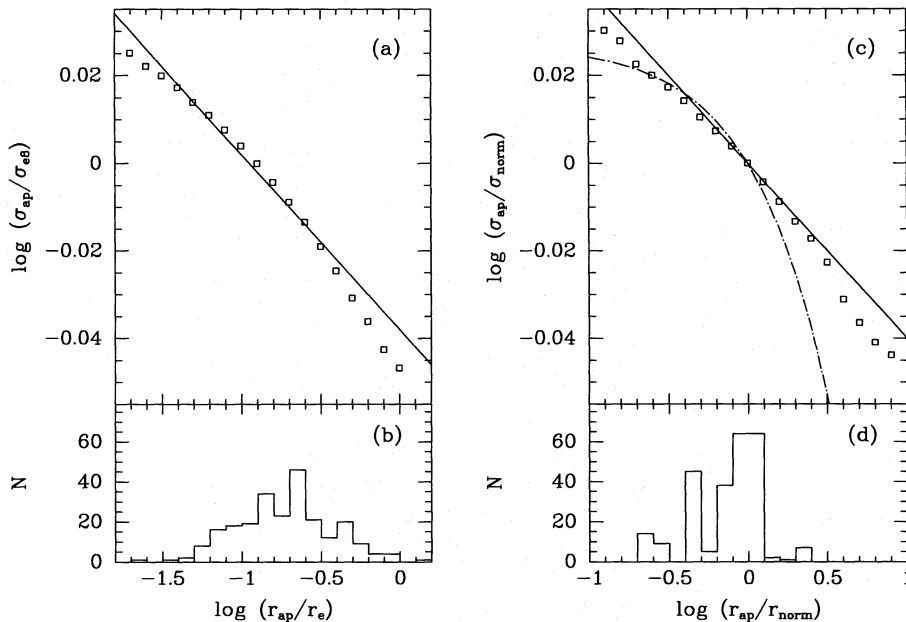
Figure 4. The dependence of the velocity dispersion on aperture size. (a) The velocity dispersion σ_{ap} has been normalized to that measured through an aperture with radius $r_e/8$. The points show the median values for our empirical models of galaxies. The line is a power-law fit, with a slope of -0.04. It provides a very good fit. (b) Distribution of r_{ap}/r_e for our data. We used an aperture radius of $r_e/8$ to correct our data. (c) The velocity dispersion has been normalized to that measured through an aperture with a metric diameter $2r_{norm} = 1.19 \ h^{-1}$ kpc. The solid line is the power-law fit with a slope of -0.04. The dot-dashed line is the correction used by Davies et al. (1987). (d) Distribution of r_{ap}/r_{norm} for our data. We used $2r_{norm} = 1.19 \ h^{-1}$ kpc to correct the velocity dispersions.

substituted for $\log \sigma$ in equation (4). The individual measurements of velocity dispersion and Mg_2 were corrected to a standard aperture with diameter $2\,r_{norm} = 1.19\ h^{-1}$ kpc. The values are presented in the Appendix. Mean values for all galaxies are given in Table 4. This table also lists velocity dispersions and Mg_2 corrected to $r_{norm} = r_e/8$.

5.3 Velocity dispersion correction of Mg_2

The mean Mg_2 indices were corrected for the effect of the velocity dispersion. We established the correction from K-giant spectra. The star spectra were first convolved to the Lick/IDS instrumental dispersion and then convolved with Gaussians with σ spanning velocity dispersions from 50 to 350 km s^{-1}. The difference between the Mg_2 index for the unconvolved spectra and the convolved spectrum as a function of the input velocity dispersion was fitted with a low-order polynomial. For a velocity dispersion of 250 km s^{-1}, the correction is 0.003. The effect of the velocity dispersion is to weaken the Mg_2 index. Thus, the correction was added to the indices in order to correct the indices to zero velocity dispersion. The size and the sign of the correction agree with the correction established by Davies et al. (1993).

6 INTERNAL AND EXTERNAL COMPARISONS

6.1 Velocity dispersions

6.1.1 Internal consistency

Internal comparisons of the velocity dispersions are shown in Figs 5(a)–(c). Table 6 summarizes the comparisons. Before the comparisons were made, the velocity dispersions were aperture-corrected to $2\,r_{norm} = 1.19\ h^{-1}$ kpc.

The scatter for the B&C comparison agrees with the formal uncertainty. The scatter for the comparisons that involve OPTOPUS observations is slightly larger than expected from the formal uncertainties. The offset between the velocity dispersions derived from B&C spectra from OPTOPUS spectra is, at the 2σ level, $\log \sigma_{B\&C} - \log \sigma_{OPTOPUS} = 0.035 \pm 0.018$, based on the five galaxies in common that have S/N larger than 20 for both observations. The same offset is found for all 10 galaxies in common.

To check further the consistency of the velocity dispersions derived from B&C and from OPTOPUS spectra, we have compared our results with determinations by Lucey & Carter (1988). We have observed 20 galaxies with B&C and 24 galaxies with OPTOPUS in common with Lucey & Carter. We aperture-corrected the velocity dispersions from Lucey & Carter to $2\,r_{norm} = 1.19\ h^{-1}$ kpc. The comparison is shown in Fig. 5(d). Our determinations of velocity dispersions $\lesssim 100$ km s^{-1} are systematically smaller than the determinations from Lucey & Carter. The effect seems to depend on the S/N of the spectra, which is reflected as the size of the error bars in the figure. Above $\log \sigma = 2.0$, the effect is marginal. For B&C observations with S/N ≥ 20 and $\log \sigma \geq 2.0$ (13 galaxies), the mean difference $\log \sigma_{our} - \log \sigma_{L\&C}$ is -0.008 ± 0.017, with an rms scatter of 0.062. For OPTOPUS observations with S/N ≥ 20 and $\log \sigma \geq 2.0$ (18 galaxies), the mean difference is -0.021 ± 0.012 with an rms scatter of 0.049. The resulting offset is $\log \sigma_{B\&C} - \log \sigma_{OPTOPUS} = 0.013$. Thus, the mean of the offset derived directly for our data and this offset is 0.024. We added 0.024 to the OPTOPUS determinations of $\log \sigma$ and then derived the final mean values (see Table 4). We adopt an uncertainty of 0.011 on the offset, since this is the difference between the mean offset and each of the determinations.

Table 4. Spectroscopic parameters (mean values).

Galaxy	cz_{hel}	$\log \sigma$ (3″4)	$\log \sigma$ ($r_e/4$)	$\sigma_{\log \sigma}$	Mg_2 (3″4)	Mg_2 ($r_e/4$)	σ_{Mg_2}	N_{obs}
A194:								
D52	6306	1.876[a]	1.901	0.041	0.206	0.231	0.011	2
I0120	4806	2.040[a]	2.054	0.053	0.247	0.262	0.017	1
I1696	5827	2.186	2.203	0.022	0.296	0.313	0.007	1
N0533	5606	2.412[a]	2.400	0.032	0.322	0.310	0.011	1
N0535	4906	2.111[a]	2.118	0.046	0.242	0.249	0.015	1
N0541	5453	2.283	2.281	0.030	0.301	0.300	0.009	1
N0545	5332	2.364	2.359	0.014	0.308	0.303	0.005	2
N0547	5546	2.394	2.401	0.013	0.323	0.330	0.005	2
N0548	5410	2.092	2.100	0.035	0.246	0.254	0.010	1
N0560	5510	2.254	2.265	0.015	0.283	0.293	0.005	2
N0564	5836	2.355	2.361	0.022	0.294	0.300	0.007	1
ZH07	5785	2.181	2.203	0.026	0.254	0.277	0.009	1
ZH09	5535	2.085	2.106	0.026	0.244	0.265	0.008	1
ZH10	5296	2.321	2.345	0.027	0.315	0.340	0.010	1
ZH12	5237	2.211	2.231	0.019	0.259	0.279	0.007	1
ZH19	4489	2.052	2.066	0.025	0.233	0.247	0.007	1
ZH31	5939	1.833	1.854	0.037	0.193	0.215	0.009	2
ZH39	4853	2.280	2.298	0.019	0.270	0.289	0.006	1
ZH52	5592	2.011	2.036	0.043	0.297	0.322	0.010	1
ZH53	5712	1.934[a]	1.947	0.039	0.201	0.214	0.010	1
ZH56	8269	2.328	2.348	0.018	0.308	0.328	0.006	1
A539:								
D16	9695	2.295	2.301	0.030	0.289	0.295	0.010	1
D22	13041	2.134	2.144	0.034	0.194	0.204	0.008	1
D23	12242	2.074[a]	2.084	0.064	0.210	0.220	0.014	1
D29	8529	2.118	2.128	0.040	0.252	0.262	0.009	1
D31	8742	2.200	2.199	0.021	0.242	0.241	0.006	1

Table 4 – *continued*

Galaxy	cz_{hel}	$\log \sigma$ (3"/4)	$\log \sigma$ (r_e/4)	$\sigma_{\log \sigma}$	Mg_2 (3"/4)	Mg_2 (r_e/4)	σ_{Mg_2}	N_{obs}
D35	8063	2.284	2.294	0.022	0.289	0.299	0.007	1
D36	8382	2.087	2.097	0.031	0.278	0.288	0.009	1
D37	9838	2.251	2.261	0.017	0.284	0.294	0.006	1
D38	9209	2.238	2.238	0.022	0.269	0.269	0.007	1
D39	8634	2.226	2.231	0.018	0.263	0.268	0.005	1
D41	8129	2.203	2.223	0.025	0.262	0.282	0.007	1
D42	8677	2.176	2.182	0.022	0.265	0.271	0.007	1
D43	8410	2.091	2.096	0.029	0.199	0.204	0.008	1
D44	7429	2.298	2.311	0.013	0.273	0.286	0.004	1
D45	8708	2.354	2.364	0.015	0.316	0.327	0.005	1
D48	7741	2.269	2.303	0.019	0.296	0.330	0.006	1
D50	8675	2.355	2.372	0.017	0.293	0.309	0.005	1
D51	9363	2.221	2.234	0.018	0.263	0.276	0.006	1
D52	8079	2.145	2.168	0.030	0.269	0.292	0.008	1
D53	6664	2.384	2.397	0.016	0.275	0.288	0.005	1
D54	8838	2.138	2.148	0.024	0.255	0.265	0.007	1
D57	10012	2.247	2.257	0.024	0.301	0.311	0.007	1
D59	7210	2.232	2.233	0.023	0.279	0.280	0.006	1
D60	9753	2.408	2.411	0.018	0.269	0.272	0.006	1
D61	7879	2.156	2.186	0.023	0.269	0.299	0.007	1
D62	9292	2.276	2.283	0.019	0.280	0.288	0.006	1
D63	7101	2.261	2.272	0.015	0.236	0.248	0.004	1
D64	8672	2.170	2.173	0.021	0.230	0.232	0.006	1
D68	9699	2.512	2.510	0.013	0.338	0.335	0.004	1
D69	9931	2.379	2.413	0.021	0.304	0.338	0.006	1
D75	9100	2.117	2.143	0.026	0.282	0.308	0.008	1
D76	7962	2.160	2.170	0.042	0.207	0.217	0.010	1
D78	9361	2.231	2.241	0.025	0.259	0.269	0.008	1
A3381:								
D19	12048	1.897a	1.905	0.082	0.162	0.170	0.014	1
D20	11523	1.980	1.988	0.041	0.185	0.193	0.008	1
D21	11311	2.294	2.302	0.017	0.303	0.312	0.005	1
D25	11495	2.306	2.300	0.023	0.288	0.282	0.009	1
D28	10954	2.146	2.154	0.024	0.254	0.262	0.006	1
D33	11692	2.292	2.308	0.019	0.237	0.254	0.007	1
D34	11355	2.376	2.380	0.034	0.244	0.248	0.010	2
D37	11154	1.981a	1.995	0.058	0.210	0.223	0.011	1
D46	8981	2.068	2.076	0.049	0.218	0.226	0.010	1
D47	8755	1.909	1.917	0.050	0.156	0.164	0.007	1
D48	8900	2.180	2.188	0.020	0.249	0.257	0.005	1
D50	11226	2.111	2.120	0.041	0.248	0.256	0.008	1
D55	11557	2.336	2.326	0.018	0.322	0.312	0.006	1
D56	11306	2.342	2.349	0.030	0.309	0.316	0.009	1
D64	11487	2.138a	2.154	0.061	0.187	0.204	0.014	1
D67	11255	2.063a	2.089	0.058	0.251	0.278	0.013	1
D68	11335	2.194a	2.203	0.037	0.283	0.293	0.014	1
D69	10375	2.060a	2.068	0.074	0.196	0.204	0.014	1
D72	10956	1.856a	1.864	0.108	0.175	0.183	0.016	1
D73	11213	2.125a	2.135	0.084	0.243	0.253	0.020	1
D75	11463	2.339	2.346	0.026	0.269	0.276	0.008	1
D76	15106	2.285a	2.293	0.046	...	...	...	1
D91	9178	1.959a	1.967	0.089	0.225	0.233	0.018	1
D100	11488	2.310a	2.315	0.028	0.284	0.289	0.011	1
D112	11059	2.347a	2.342	0.029	0.288	0.282	0.011	1
A3574:								
W22	4585	2.330	2.346	0.017	0.308	0.324	0.006	1

Galaxy	cz_{hel}	$\log \sigma$ (3"/4)	$\log \sigma$ (r_e/4)	$\sigma_{\log \sigma}$	Mg_2 (3"/4)	Mg_2 (r_e/4)	σ_{Mg_2}	N_{obs}
W39	5095	2.166	2.156	0.021	0.259	0.249	0.008	1
W47	4560	2.392	2.380	0.018	0.325	0.314	0.006	1
W60	3763	2.349	2.350	0.022	0.261	0.262	0.007	1
W69	5405	1.935	1.949	0.026	0.170	0.183	0.006	1
W74	4251	2.320	2.342	0.017	0.299	0.321	0.007	1
W81	4571	2.271	2.279	0.019	0.289	0.297	0.007	1
S639:								
E264G23	5658	2.342	2.339	0.018	...	...	...	1
E264G24	6099	2.349	2.357	0.010	0.273	0.281	0.003	2
E264G26	6339	2.115	2.123	0.025	0.243	0.251	0.007	1
E264G28	6603	2.191	2.199	0.017	0.242	0.250	0.005	1
E264G300	6140	2.449	2.451	0.023	0.315	0.317	0.008	1
E264G301	5358	2.265	2.284	0.015	0.280	0.299	0.011	2
E264G302	6482	2.276	2.298	0.022	0.262	0.284	0.006	1
E264G31	6694	2.392	2.388	0.014	0.283	0.279	0.005	1
J06	6470	2.041	2.048	0.040	0.201	0.207	0.009	1
J09	6253	1.852a	1.860	0.105	0.210	0.218	0.018	1
J10	6814	1.856a	1.865	0.061	0.192	0.200	0.011	1
J13	6627	2.298	2.311	0.013	0.263	0.276	0.004	2
J14	5682	2.135	2.143	0.023	...	...	...	1
J15	5854	2.105	2.132	0.020	...	...	...	1
J16	5925	2.094	2.115	0.027	...	...	...	1
J18	5959	1.935a	1.943	0.077	...	...	...	1
J20	5546	1.633a	1.641	0.134	...	...	...	1
J23	6367	2.140	2.170	0.034	0.249	0.279	0.009	1
J26	6663	2.496	2.504	0.019	0.303	0.312	0.006	1
J31	5805	1.715a	1.723	0.159	...	...	...	1
J32	6536	2.187	2.195	0.017	0.267	0.275	0.005	1
J101	7085	1.960	1.969	0.042	0.210	0.218	0.010	1
J104	6547	2.018	2.026	0.068	0.137	0.145	0.010	1
J109	6956	2.154	2.162	0.019	0.252	0.260	0.006	1
S753:								
W08	3966	2.055	2.047	0.020	0.234	0.226	0.008	1
W10	3962	2.100	2.127	0.017	0.226	0.254	0.006	1
W12	4169	2.201	2.222	0.018	0.282	0.303	0.007	1
W17	4175	1.993	2.016	0.026	0.197	0.220	0.008	1
W26	3449	2.154	2.163	0.018	0.245	0.254	0.007	1
W29	4161	2.420	2.431	0.024	0.305	0.316	0.008	1
W37	3924	2.222	2.247	0.020	0.298	0.323	0.006	1
W39	10630	2.332	2.354	0.028	0.280	0.303	0.009	1
W47	4266	2.067	2.089	0.031	0.249	0.271	0.010	1
W49	5135	2.387	2.420	0.019	0.302	0.335	0.006	1
W51	4026	2.171	2.188	0.024	0.247	0.263	0.009	1
W54	4697	2.248	2.259	0.018	0.260	0.271	0.006	1
W64	4193	2.522	2.512	0.017	0.335	0.325	0.005	2
W73	3849	2.260	2.271	0.019	0.301	0.312	0.007	1
W84	4498	2.318	2.337	0.024	0.294	0.313	0.009	1
W95	4659	2.108	2.125	0.020	0.259	0.275	0.007	1
DC2345-28:								
D38	9049	2.070a	2.086	0.054	0.296	0.312	0.017	1
Doradus:								
A0426-54	1547	1.653	1.669	0.102	0.086	0.101	0.009	1
N1411	1022	2.099	2.126	0.013	0.213	0.240	0.004	2
N1527	1199	2.198	2.217	0.012	0.260	0.279	0.004	2
N1533	821	2.243	2.265	0.024	0.282	0.305	0.009	1
N1543	1202	2.158	2.176	0.014	0.277	0.296	0.005	2

Table 4 – *continued*

Galaxy	cz_{hel}	$\log\sigma$ (3″4)	$\log\sigma$ $(r_e/4)$	$\sigma_{\log\sigma}$	Mg_2 (3″4)	Mg_2 $(r_e/4)$	σ_{Mg_2}	N_{obs}
N1549	1259	2.293	2.308	0.018	0.263	0.278	0.006	1
N1553	1247	2.215	2.220	0.020	0.264	0.269	0.007	1
N1574	1030	2.313	2.337	0.020	0.287	0.310	0.008	1
N1596	1534	2.196	2.220	0.016	0.271	0.294	0.005	1
Grm15:								
A1959-56	4464	2.419	2.412	0.024	0.332	0.325	0.009	1
I4944	5890	2.080	2.083	0.041	0.159	0.161	0.008	1
I4952	4289	2.123	2.127	0.030	0.225	0.229	0.008	1
N6848	4447	2.256	2.246	0.021	0.240	0.229	0.008	3
N6850	4906	2.248	2.252	0.013	0.224	0.229	0.005	1
N6854	5747	2.328	2.324	0.019	0.301	0.297	0.005	1
N6855	4426	2.282	2.286	0.040	0.320	0.324	0.007	1
HydraI – A1060:								
E436G44	3165	2.213	2.229	0.024	0.258	0.273	0.009	1
E436G45	3402	2.279	2.314	0.028	0.268	0.303	0.010	1
E437G11	4938	2.275	2.292	0.015	...	...	...	1
E437G13	3499	2.224	2.246	0.012	...	...	...	1
E437G21	3931	2.248	2.261	0.019	0.283	0.296	0.008	1
E437G45	3757	2.103[a]	2.114	0.031	0.279	0.290	0.014	1
E501G03	4199	2.323	2.332	0.018	0.285	0.294	0.008	2
E501G13	3520	2.352	2.369	0.021	0.306	0.322	0.009	1
E501G27	3230	1.739	1.763	0.072	...	...	...	1
E501G35	4181	2.172	2.188	0.010	...	...	...	1
E501G47	4838	2.135	2.154	0.015	...	...	...	1
E501G49	4063	2.036	2.059	0.022	...	...	...	1
I0629	2822	2.058	2.075	0.020	...	...	...	1
I2597	2971	2.388	2.389	0.013	0.318	0.319	0.007	2
N3305	3976	2.391	2.407	0.010	...	...	...	1
N3308	3568	2.288	2.284	0.011	0.303	0.299	0.011	2
N3309	4094	2.418	2.420	0.009	0.336	0.337	0.011	2
N3311	3868	2.291	2.265	0.015	0.332	0.307	0.012	2
N3315	3793	2.211	2.222	0.015	...	...	...	1
N3316	3876	2.228	2.236	0.012	...	...	...	1
R213	3583	1.997	2.024	0.017	...	...	...	1
R219	4188	2.023	2.047	0.022	...	...	...	1
R224	3764	2.013	2.036	0.033	...	...	...	1
R225	3522	1.937	1.965	0.031	...	...	...	1
R231	3685	1.942	1.976	0.031	...	...	...	1
R245	4789	2.068	2.084	0.020	...	...	...	1
R253	4686	1.904	1.922	0.034	...	...	...	1
R254	4662	1.750	1.779	0.074	...	...	...	1
R261	3807	1.661[a]	1.691	0.098	...	...	...	1
R293	4482	1.816[a]	1.841	0.079	...	...	...	1
R303	2758	1.643[a]	1.671	0.124	...	...	...	1
R308	4103	1.967	1.986	0.037	...	...	...	1
R319	4460	2.086	2.117	0.027	...	...	...	1
R327	4213	1.966	1.992	0.045	...	...	...	1
R338	4372	1.750	1.779	0.074	...	...	...	1
RMH26	2286	2.024	2.043	0.019	...	...	...	1
RMH28	3006	2.148	2.170	0.020	0.273	0.295	0.011	2
RMH29	3441	2.184	2.213	0.018	...	...	...	1
RMH30	10672	2.286	2.294	0.021	0.272	0.280	0.007	1
RMH35	4739	2.090	2.112	0.015	...	...	...	1
RMH50	3075	1.963	1.984	0.022	...	...	...	1
RMH72	4895	2.076	2.103	0.014	0.250	0.277	0.010	2
RMH79	2687	2.268	2.287	0.015	...	...	...	1
Hickson groups:								
H86A	6062	2.398	...	0.024	0.336	...	0.008	1
H86B	5837	2.313	...	0.026	0.288	...	0.008	1
H86C	5317	2.239[a]	...	0.036	0.307	...	0.015	1
H86D	6019	2.274	...	0.025	0.286	...	0.007	1
H90B	2551	2.410	...	0.023	0.318	...	0.009	1
H90C	2600	2.266	...	0.019	0.285	...	0.007	1
H90D	2711	2.132	...	0.032	0.185	...	0.009	1
H98A	7947	2.396	...	0.020	0.289	...	0.007	1
H98B	7999	2.390	...	0.023	0.305	...	0.008	1
Other:								
E462G15	5844	2.459	2.456	0.026	0.292	0.289	0.009	1
E553G02	4814	2.406[a]	2.408	0.060	0.279	0.281	0.020	1
I2006	1388	2.070	2.086	0.015	0.262	0.278	0.005	2
N0720	1722	2.373	2.373	0.015	0.326	0.337	0.005	1
N1339	1332	2.205	2.232	0.019	0.296	0.323	0.007	1
N1395	1698	2.375	2.381	0.018	0.316	0.323	0.006	1
N1399	1454	2.535	2.544	0.022	0.331	0.339	0.008	1
N1403	4282	2.199	2.210	0.024	0.250	0.260	0.009	2
N1426	1422	2.170	2.190	0.020	0.251	0.271	0.007	1
N1439	1679	2.120	2.137	0.019	0.282	0.299	0.008	2
N1600	4760	2.472	2.458	0.030	0.334	0.320	0.011	1
N1726	3989	2.387	2.389	0.016	0.291	0.292	0.007	1
N1794	5002	2.270	2.273	0.030	0.218	0.222	0.008	1
N2293	2025	2.397	2.405	0.014	0.308	0.315	0.006	2
N2513	4728	2.469	2.468	0.026	0.314	0.312	0.010	1
N2865	2651	2.216	2.229	0.018	0.199	0.211	0.006	1
N2974	1921	2.408	2.418	0.013	0.291	0.301	0.005	2
N2986	2319	2.381	2.386	0.015	0.325	0.330	0.005	2
N3377	716	2.132	2.147	0.013	0.242	0.258	0.004	1
N3379	912	2.300	2.315	0.015	0.304	0.319	0.005	1
N5898	2157	2.362	2.372	0.012	0.300	0.310	0.004	2
N5903	2556	2.292	2.295	0.016	0.281	0.284	0.006	1
N6849	6100	2.301	2.290	0.026	0.272	0.261	0.009	1
N7619	3793	2.472	2.471	0.016	0.329	0.329	0.005	1
N7626	3405	2.423	2.420	0.017	0.315	0.312	0.006	1

Notes. $\log\sigma$ and Mg_2 have been aperture-corrected. Mg_2 is transformed to the Lick system, and corrected to zero velocity dispersion. cz_{hel} – the heliocentric radial velocity. $\sigma_{\log\sigma}$ – the formal uncertainty on $\log\sigma$ as derived from the fit. (3″4) – aperture-corrected to $2r_{norm} = 1.19\ h^{-1}$ kpc, equivalent to 3.4 arcsec at the distance of the Coma cluster. $(r_e/4)$ – aperture-corrected to $2r_{norm} = r_e/4$.

The effective radii, r_e, were taken from Jørgensen et al. (1995a). For galaxies in A539, A3381 and S639, which are not included in this paper, the median effective radius for galaxies in the cluster was used: $\log r_e = 0.788, 0.719$ and 0.960, respectively. For galaxies in HydraI not included in Jørgensen et al. (1995a), we used $\log r_e = 1.23 \log r_{25} - 0.99$, where r_{25} is from Richter (1989).

[a]$S/N < 20$, $\log\sigma$ subject to systematic errors. Values of $\log\sigma$ below 2.0 may also be subject to systematic errors.

Table 5. Spectroscopic parameters from the literature.

Galaxy	log σ (3".4)	(re/4)	Mg2 (3".4)	(re/4)	Galaxy	log σ (3".4)	(re/4)	Mg2 (3".4)	(re/4)
A194:					D125	2.231	2.267	0.273	0.309
N0538	2.305	2.310	...	...	D128	2.037	2.065	0.259	0.287
ZH05	2.161	2.179	...	...	D129	2.404	2.376	0.325	0.298
ZH08	2.074	2.090	...	...	D130	2.328	2.352	0.305	0.330
ZH48	1.873	1.889	...	...	D131	2.243	2.251	0.290	0.298
DC2345-28:					D132	2.122	2.142	0.272	0.292
D32	2.465	2.473	0.333	0.341	D133	2.350	2.375	0.312	0.337
D33	1.912	1.927	...	...	D135	1.901	1.920	...	...
D37	1.949	1.963	...	...	D136	2.184	2.221	0.280	0.317
D38	2.207	2.228	...	...	D137	2.227	2.245	0.272	0.290
D39	2.122	2.134	...	...	D143	2.348	2.344	0.335	0.330
D40	1.913	1.927	...	...	D144	2.228	2.238	0.283	0.293
D42	2.337	2.327	0.364	0.355	D145	2.142	2.152	0.292	0.302
D43	2.269	2.273	...	...	D146	2.039	2.042	0.255	0.258
D44	2.201	2.243	0.294	0.336	D148	2.587	2.572	0.354	0.339
D45	2.094	2.109	0.244	0.259	D150	2.027	2.044	0.285	0.302
D49	2.098	2.121	...	...	D151	2.178	2.184	0.253	0.259
D50	2.305	2.310	...	...	D152	2.210	2.217	0.281	0.288
D51	2.179	2.210	...	...	D153	2.132	2.153	0.285	0.307
D52	1.806	1.822	0.237	0.253	D155	2.193	2.203	0.292	0.302
D53	1.842	1.872	...	...	D156	2.001	2.025	0.235	0.259
D55	2.219	2.239	0.306	0.327	D157	2.118	2.142	0.260	0.284
D56	2.420	2.415	0.312	0.307	D159	2.297	2.306	0.290	0.299
D58	2.411	2.419	0.294	0.303	D160	2.276	2.284	0.309	0.317
D59	2.224	2.237	...	...	D161	2.242	2.251	0.306	0.315
D60	2.089	2.107	0.253	0.271	D167	2.325	2.336	0.274	0.285
D65	2.329	2.330	...	...	D168	2.328	2.347	0.310	0.329
D66	2.030	2.051	...	...	D170	2.164	2.174	0.298	0.308
D67	2.008	2.018	...	...	D172	2.204	2.227	0.304	0.328
D68	2.092	2.123	...	...	D173	2.156	2.179	0.296	0.319
D69	1.913	1.908	...	...	D174	2.257	2.287	0.296	0.327
D70	2.131	2.168	0.288	0.325	D175	2.252	2.263	0.306	0.317
D76	2.138	2.155	...	...	D176	2.225	2.249	0.291	0.315
D77	2.309	2.316	...	...	D177	2.016	2.038	0.265	0.287
D83	2.104	2.113	...	...	D179	2.388	2.404	0.294	0.310
Coma:					D181	2.170	2.194	0.257	0.281
D24	2.347	2.366	0.305	0.324	D191	1.965	1.994	0.256	0.285
D27	1.997	2.015	0.264	0.282	D192	1.975	1.989	0.231	0.245
D31	2.429	2.416	0.317	0.304	D193	2.081	2.101	0.269	0.289
D46	2.370	2.383	0.323	0.336	D194	2.390	2.398	0.347	0.355
D49	2.414	2.418	0.324	0.328	D204	2.102	2.116	0.272	0.286
D57	2.225	2.232	0.275	0.282	D206	2.346	2.351	0.301	0.306
D58	2.263	2.263	0.313	0.312	D207	2.172	2.192	0.271	0.291
D65	2.079	2.091	0.261	0.273	D210	2.225	2.246	0.274	0.295
D67	2.187	2.215	0.286	0.314	D217	2.314	2.317	0.299	0.302
D68	2.129	2.138	0.278	0.287	D238	2.013	2.041	0.240	0.268
D69	2.284	2.299	0.311	0.326	D239	2.351	2.359	0.298	0.306
D70	2.180	2.199	0.296	0.316	D240	2.420	2.415	0.322	0.318
D72	2.142	2.165	0.282	0.305					
D78	2.286	2.293	0.309	0.316					
D81	2.171	2.183	0.269	0.281					
D87	1.901	1.925	0.234	0.258					
D88	2.418	2.443	0.327	0.352					
D98	2.184	2.200	0.275	0.291					
D101	2.118	2.140	0.278	0.300					
D103	2.337	2.356	0.308	0.327					
D104	2.278	2.301	0.299	0.322					
D105	2.313	2.323	0.321	0.331					
D106	2.219	2.247	0.250	0.278					
D107	1.838	1.852	0.238	0.253					
D108	2.082	2.105	0.281	0.304					
D109	2.261	2.276	0.345	0.360					
D116	2.132	2.143	0.256	0.267					
D118	2.227	2.237	0.310	0.319					
D119	2.204	2.223	0.289	0.308					
D120	2.151	2.164	0.264	0.278					
D121	2.308	2.340	0.275	0.307					
D122	1.975	1.992	0.235	0.252					
D124	2.261	2.277	0.251	0.267					

Notes. A194: Lucey & Carter (1988). DC2345−28: Lucey & Carter (1988) and Davies et al. (1987). Coma: Davies et al. (1987), Dressler (1987), Lucey et al. (1991) and Guzmán et al. (1992). The parameters have been offset to consistency with Davies et al. (1987), aperture-corrected and averaged.
$\log \sigma$ (Davies et al.) = $\log \sigma$ (Lucey & Carter) $-0.020 = \log \sigma$ (Dressler) $+0.013 = \log \sigma$ (Lucey et al.) -0.030. Mg2 (Davies et al.) = Mg2 (Dressler) $+0.002 =$ Mg2 (Guzmán et al.) $+0.010$.
(3".4) – aperture corrected to $2r_{norm} = 1.19\ h^{-1}$ kpc, equivalent to 3.4 arcsec at the distance of the Coma cluster. ($r_e/4$) – aperture-corrected to $2r_{norm} = r_e/4$. The effective radii, r_e, are given in Jørgensen et al. (1995a).

We have checked if the difference in wavelength interval between B&C observations and OPTOPUS observations could cause the offset. Velocity dispersions were derived from B&C observations from the same wavelength interval as was available for the OPTOPUS observations. This did not change the results significantly. Thus, the offset cannot be ascribed to the difference in wavelength interval. It should be noted that the B&C spectra and the OPTOPUS spectra

were taken with two different spectrographs, although both are Boller & Chivens spectrographs. Also, different gratings were used for the observations. We discuss the possible origin of offsets between different sets of data further in Section 6.1.2.
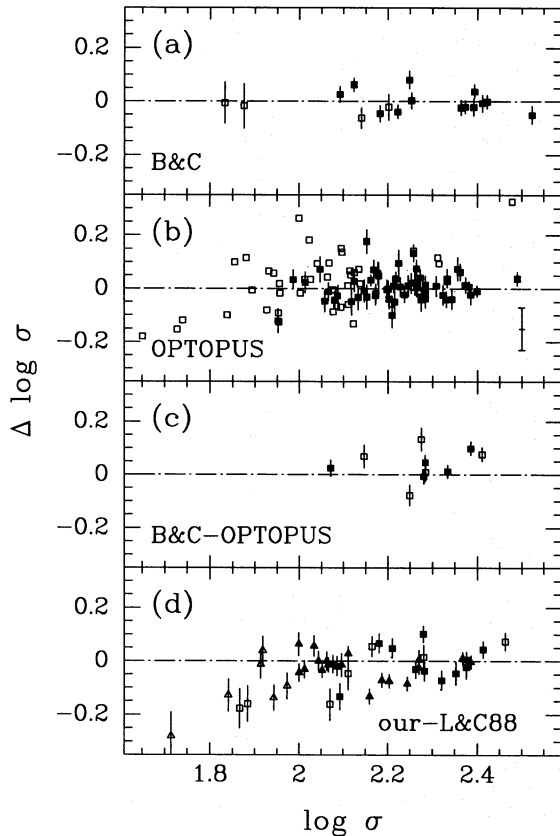

Figure 5. Internal consistency of the derived velocity dispersion. All data shown in this figure have been aperture-corrected with our aperture correction. The error bars are the formal uncertainties. (a)–(c) Internal comparisons: solid symbols – observations with $S/N \geq 20$; open symbols – observations with $S/N < 20$ for one or both observations. The error bar in the lower right corner of panel (b) applies to the open symbols. (d) Comparison of velocity dispersions with data from Lucey & Carter (1988). Boxes – our B&C observations; triangles – our OPTOPUS observations. Solid symbols – $\log \sigma \geq 2.0$ and $S/N \geq 20$ for our observation; open symbols – $\log \sigma < 2.0$ or $S/N < 20$ for our observation. The error bars include our formal uncertainties as well as the uncertainties on the data from Lucey & Carter.

For velocity dispersions below 100 km s^{-1}, we find a mean offset $\log \sigma_{our} - \log \sigma_{L\&C} = -0.12$. Velocity dispersions derived from spectra with $S/N < 20$ have a mean offset relative to the data from Lucey & Carter of -0.067. The velocity dispersions derived from low S/N spectra and velocity dispersions smaller than 100 km s^{-1} may have a systematic error of ≈ 20 per cent. Thus, the general conclusion from this comparison agrees with our simulations of the effects of noise (cf. Section 5.1). Because we cannot simulate the observations by Lucey & Carter in detail, we are not able to quantify the effect further. Measurements based on low S/N spectra are marked in Table 4.

6.1.2 Comparison with published results

The mean velocity dispersions were compared with data published by Davies et al. (1987), Lucey & Carter (1988) and Whitmore, McElroy & Tonry (1985). The velocity dispersions from the literature were aperture-corrected to $2 r_{norm} = 1.19 \, h^{-1}$ kpc. Our aperture-corrected mean values (Table 4) were then compared with the data from the literature. Fig. 6 shows the comparisons, and Table 7 summarizes the offsets and the rms scatter for the differences. All differences are calculated as 'our'–'literature'.

We compared our mean velocity dispersions with the individual measurements published by Davies et al. (1987). The comparisons with the Lick data and the KPNO data each have a significantly higher rms scatter than the rest of the comparisons. The Lick data have rather low spectral resolution, and the KPNO data are undersampled relative to the formal spectral resolution. This may cause the higher scatter. The comparisons show that the data from Davies et al. are of rather inhomogeneous quality, with the LCOLO and LCOHI data being of significantly higher accuracy than the other data. If we use the typical uncertainty on single Lick measurements given by Davies et al. (0.057 on $\log \sigma$), and for the other comparisons assume the uncertainties to be equally distributed on the two data sets, we find a typical rms error on our measurements of 0.036 in $\log \sigma$. The KPNO data have been excluded in this estimate. The estimated rms error is of the same size as the error estimated by Davies et al. for those data that do not originate from the Lick observations.

None of the offsets relative to the velocity dispersions from Davies et al. are significant. Thus, our data are on a system consistent with Davies et al. We confirmed this by comparing our measurements with the mean values of the aperture-corrected individual measurements from Davies et al. (our aperture correction). Our determination of the

Table 6. Internal comparison of spectroscopic parameters.

Obs.run	Number of observations	rms of Δcz_{hel}	rms of $\Delta \log \sigma$	rms of ΔMg_2	remark
B&C	17	22	0.039	0^m019	All
B&C	13	23	0.041	0^m021	$S/N \geq 20$
OPTOPUS	98	22	0.082	0^m021^a	All
OPTOPUS	56	20	0.052	0^m014^b	$S/N \geq 20$
B&C – OPTOPUS	10	51	0.060	0^m007^c	All
B&C – OPTOPUS	5	67	0.040	$\cdots$	$S/N \geq 20$

[a] 56 galaxies in common. [b] 32 galaxies in common. [c] 3 galaxies in common.
$\log \sigma$ and Mg_2 were aperture-corrected to $2 r_{norm} = 1.19 \, h^{-1}$ kpc before comparison.
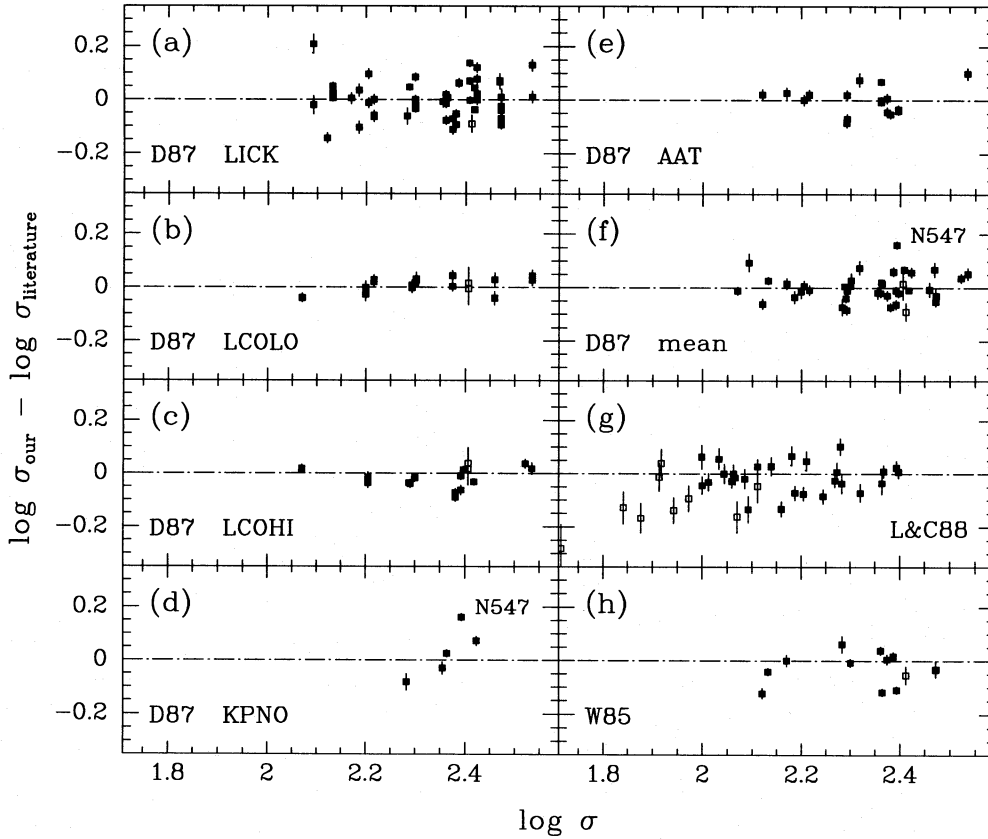
Figure 6. Comparison of our velocity dispersions with data from the literature. Both the literature data and our data have been aperture-corrected to a circular aperture with metric diameter 1.19 h^{-1} kpc. Solid boxes – observations with S/N $\geq$ 20 and log $\sigma \geq$ 2.0; open boxes – observations with S/N < 20 or log σ < 2.0. (a)–(e) Individual measurements from Davies et al. (1987). The origin of the literature data are given in the panels with the same coding as used by Davies et al. (f) Mean values of the data from Davies et al. derived by us. (g) Lucey & Carter (1988). (h) Whitmore et al. (1985). The error bars in (a)–(f) and (h) are our formal uncertainties. The error bars in (g) include the uncertainty on the data from Lucey & Carter.

Table 7. Comparison with data from the literature.

Source	N	$< \Delta cz_{hel} >$ [km/s]	rms of Δcz_{hel}	$< \Delta \log \sigma >$	rms of $\Delta \log \sigma$	$< \Delta Mg_2 >$	rms of ΔMg_2
Davies et al. (1987)							
LICK	51			0.003	0.071		
LCOLO	20			0.009	0.028		
LCOHI	17			−0.015	0.038		
KPNO	5			0.029	0.093		
AAT	17			0.000	0.051		
mean	39	24	65	0.002	0.053	−0.014	0.020
mean[a]	36-37	16	51[b]	0.000	0.045[c]	−0.014	0.019
Faber (1994)	24					−0.008	0.017
Lucey & Carter (1988)	36	16	35	−0.038	0.080		
Lucey & Carter (1988)[a]	27	11	34	−0.017	0.058		
Whitmore et al. (1985)	14			−0.028	0.057		
Richter (1989)	40	1	99				
Dressler & Shectman (1988)	22	−4	109				
Willmer et al. (1991)	18	3	63				
Willmer et al. (1991)[d]	17	11	53				

Notes. The differences are calculated as 'our'–'literature'. log σ and Mg$_2$ were aperture-corrected to a circular aperture with diameter 1.19 h^{-1} kpc (see text).
[a]S/N $\geq$ 20 and log σ > 2.0 for our data. [b]N3311 is excluded. [c]N547 is excluded. [d]A3574 − W39 is excluded; the radial velocity for this galaxy from Willmer et al. (1991) is not obtained with the ON intensified Reticon.

velocity dispersion of the galaxy NGC 547 deviates from the result in Davies et al. The galaxy is observed only once by Davies et al. We have observed the galaxy twice, and both determinations agree with the results from Lucey & Carter (1988). The galaxy is therefore excluded from the comparison with the mean velocity dispersions from Davies et al. For the 36 galaxies in common with S/N > 20, we find for $\log \sigma$: 'our'–'Davies' = 0.000 ± 0.008 with an rms scatter of 0.045.

New observations by Dressler, Faber & Burstein (1991) indicate that the velocity dispersions from Davies et al. may be systematically too high for low-velocity-dispersion galaxies. We do not find this effect in the comparison of our data with the data from Davies et al. The comparison with data from Lucey & Carter (1988) shows a slightly larger scatter than the comparison with Davies et al. If the errors are equally distributed on the data sets, it implies a typical uncertainty on $\log \sigma$ of $\simeq 0.04$ for observations with S/N ≥ 20. Lucey & Carter found an offset of their data relative to the data from Davies et al. of 0.022, with their velocity dispersions being larger. This is consistent with the offset we find relative to the velocity dispersions from Lucey & Carter: 'our'–'their' = −0.017 ± 0.010.

We aperture-corrected the velocity dispersions from Whitmore et al. (1985) under the assumption that the observations were obtained with a 2×4 arcsec^2 slit. This is the mean slit size to which Whitmore et al. made their data consistent. The comparison shows similar scatter and offset to the comparison with Lucey & Carter.

Offsets of 0.01–0.03 in $\log \sigma$ between different sets of data have been reported in the literature, although the offsets were not always significant (Dressler 1984; Whitmore et al. 1985; Davies et al. 1987; Lucey & Carter 1988; Lucey et al. 1991). Some of these offsets can be due to differences in the aperture size. We have applied the aperture correction as described in Section 5.2 to data from Davies et al. (1987), Dressler (1987), Lucey & Carter (1988) and Lucey et al. (1991). Significant offsets of 0.01–0.03 in $\log \sigma$ are still present after the aperture correction. Our data is on the same system as the data of Davies et al. (1987), but both sets are offset from the data of Dressler, Lucey & Carter and Lucey et al. We found the following offsets for the aperture-corrected measurements: $\log \sigma$ (this paper) = $\log \sigma$(Davies et al. = $\log \sigma$ (Dressler) + 0.013 = $\log \sigma$ (Lucey & Carter) − 0.020 = $\log \sigma$ (Lucey et al.) − 0.030. These offsets were used to make all literature data used consistent (cf. footnotes to Table 5). The uncertainty on the offsets is typically 0.01 on $\log \sigma$, or about 3 per cent.

Various origins of the offsets are possible. Dressler (1984) found that velocity dispersions derived from the wavelength region around the G-band were 10 per cent smaller than velocity dispersions derived from the Mg region. Franx et al. (1989a) did not find such systematic effects in their data, and so the origin of the effect is not clear. The velocity dispersions given by Dressler (1987) are the average of determinations from the two wavelength regions, while the other authors have used 500–1000 Å, centred on the Mg lines. Spectral differences in the template stars used by different authors may be the source of offsets between measurements based on the same wavelength region. Dressler (1984) found the effect of using template stars with different metallicities to be less than 5 per cent. González

(1993) found effects of 7–8 per cent. He concludes that the reason for the systematic offsets is the failure to match the magnesium-to-iron ratio of the galaxies. However, most authors use template stars with roughly solar abundance ratios. Hence it is not clear how offsets between different sets of observations on the same galaxies can originate this way.

The mean differences between the velocity dispersions we derive with the individual template stars and the adopted mean values are of the order of 1 per cent, and are all within ± 3.5 per cent. From the results for the template stars that are common to the different observing runs, we find that the consistency of the derived velocity dispersions is within 2 per cent. We therefore find it unlikely that the offset between the velocity dispersions from the B&C spectra and those from the OPTOPUS spectra originates from the use of different template stars.

A related problem is the acquisition of the template stars itself. For long-slit observations the telescope is moved during the observation of a template star, so the signal fills the slit in the same way as for a galaxy. For the fibre observations, the telescope was not moved. Although the fibres will scramble the incoming beam, this may not be sufficient to obtain a properly filled beam at the spectrograph entrance. It is possible that the difference in the two techniques can lead to small offsets between the derived velocity dispersions.

If a consistency of better than 5 per cent of the velocity dispersions is essential, as it is for measurements of distances and peculiar velocities, we judge that it is necessary to establish and apply zero-point offsets, even to aperture-corrected measurements of the velocity dispersions.

6.2 Radial velocities

Fig. 7 shows the internal comparisons of the radial velocities. There are no significant offsets, the rms scatters for the comparisons are given in Table 6. Our determinations of the radial velocities were compared with the results from Davies et al. (1987), Dressler & Shectman (1988), Lucey & Carter (1988), Richter (1989) and Willmer et al. (1991) (see Fig. 8 and Table 7). In general the agreement is good. The rms scatters for the comparisons with data from Davies et al., Lucey & Carter and Willmer et al. show that the uncertainty on our data is $\simeq 35$ km s^{-1}. Both our determinations for NGC 3311 disagree with the value given by Davies et al. but agree with the radial velocity found by Lucey & Carter and by Richter.

6.3 The Mg$_2$ index

Fig. 9 shows the internal comparisons of the Mg$_2$ index. The indices were aperture-corrected before the comparisons were made. Table 6 gives the rms scatter for the comparisons. For the three galaxies in common, there is no significant offset between the Mg$_2$ indices derived from B&C and from OPTOPUS observations: $Mg_{2B\&C} - Mg_{2OPTOPUS} = 0.000 \pm 0.003$.

We compared our aperture-corrected mean values of Mg$_2$ with data from Davies et al. (1987) and Faber (1994, personal communication). We have re-derived the mean values for the galaxies observed by Davies et al. (1987) from the individual measurements published by these authors. The literature data were aperture-corrected with our
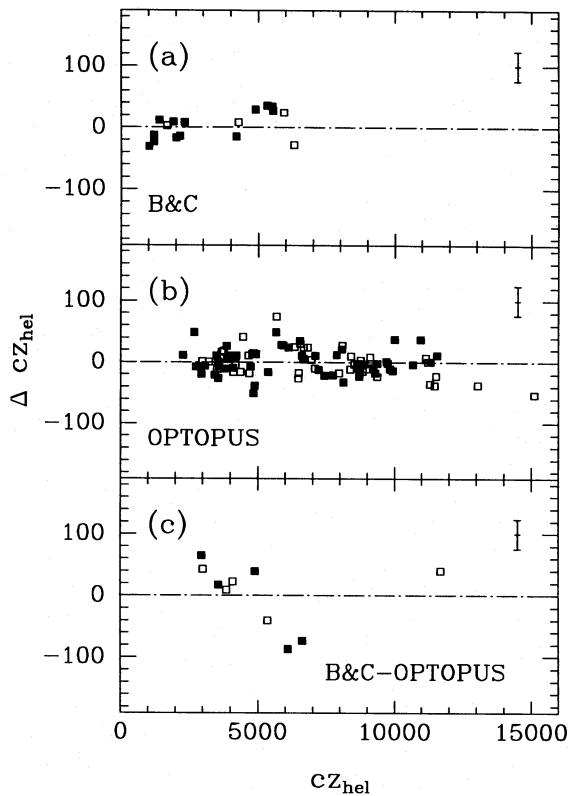
Figure 7. Internal comparisons of radial velocities. Solid boxes – observations with $S/N \geq 20$; open boxes – observations with $S/N < 20$ for one or both observations. Representative error bars for our internal uncertainties are given. The galaxies on panel (b) with $cz_{hel} < 5000$ km s^{-1} belong to the HydraI cluster. The three galaxies with cz_{hel} in the interval 5000–7000 km s^{-1} belong to S639. The apparent trend in the comparison of cz_{hel} is more likely to be an offset in the wavelength calibration of the OPTOPUS data for the two clusters.

Figure 8. Comparison of the radial velocity with data from the literature. (a) Davies et al. (1987). (b) Lucey & Carter (1988). (c) Boxes – Willmer et al. (1991); triangles – Richter (1989); circles – Dressler & Shectman (1988). Representative error bars for our internal uncertainties are given.

aperture correction. Also, the data from Faber were averaged and aperture-corrected. We assumed that all literature data were consistent with the Lick aperture size 1.5×4.0 arcsec^2 (cf. Table 3). The comparisons are shown in Fig. 10. The offsets and rms scatter are given in Table 7. The comparison with Davies et al. shows a weak trend in the sense that our Mg$_2$ indices are systematically smaller for weak-lined galaxies. The trend is not changed by applying the velocity dispersion correction to our data. Because no trend is seen in the comparison with data from Faber, we have simply adopted a zero-point offset between our values of Mg$_2$ and the Lick system: Mg$_{2inst}$ − Mg$_{2Lick}$ = − 0.011 ± 0.003. In order to reach the Lick system, we have added 0.011 to our aperture-corrected values of Mg$_2$ and then corrected the measurements for the effect of the velocity dispersion. If the errors are equally distributed on our data and the literature data, the scatter for the comparisons implies a typical uncertainty on Mg$_2$ of ± 0.013.

7 SUMMARY

We have derived central velocity dispersions, Mg$_2$ line indices and radial velocities for 220 E and S0 galaxies. The data include velocity dispersions for 151 galaxies not

previously observed, and Mg$_2$ for 134 galaxies whose line indices have not been previously measured. The observations were obtained with the ESO 1.5-m telescope, equipped with the B&C spectrograph, and with the ESO 3.6-m telescope equipped with OPTOPUS, a fibre fed multi-object spectrograph. A S/N of 25 per Å for the B&C observations gives a formal uncertainty of 6 per cent. This could be reached within 1 h with the ESO 1.5-m telescope for galaxies brighter than $B_T \approx 15$ mag. With the low read-out-noise CCD used for one of the observing runs, galaxies as faint as $B_T \approx 15.5$ mag could be observed. A S/N of 30 per Å is required for the OPTOPUS spectra in order to get a formal uncertainty of 6 per cent. The requirement of a higher S/N is partly due to the smaller wavelength range covered by this instrument. Under clear sky (which we did not have all the time) S/N = 30 can be reached with OPTOPUS in two 1-h observations for galaxies with $B_T \approx 16.5$ mag. A little more than half of our OPTOPUS observations are of this quality.

The velocity dispersions and the Mg$_2$ line indices have been corrected for the effect of the size of the aperture. The correction was established from kinematic models of the data available in the literature. The parameters were corrected to a circular aperture with metric diameter $1.19~h^{-1}$ kpc, equivalent to 3.4 arcsec at the distance of the Coma cluster. Values corrected to a circular aperture with diameter $r_e/4$ are also given. The effect of the position angle
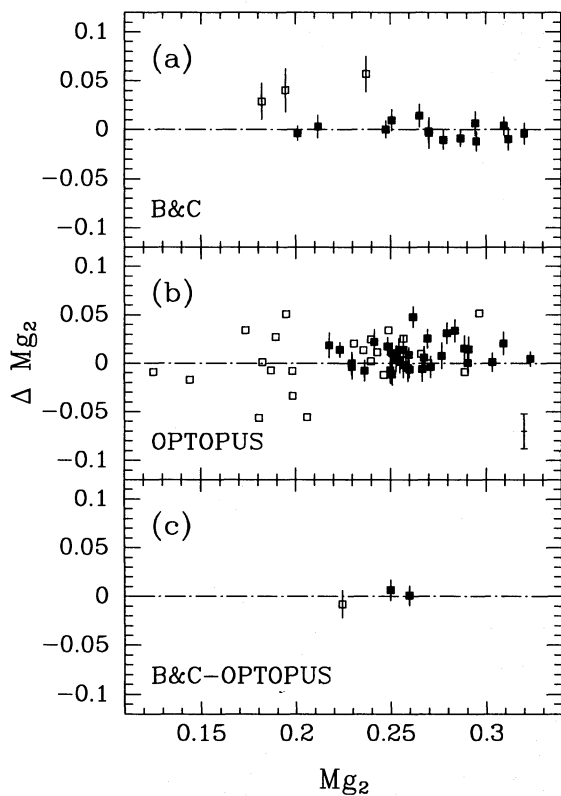
Figure 9. Internal comparison of the Mg_2 line index. The data have been aperture-corrected. Solid boxes – observations with $S/N \geq 20$; open boxes – observations with $S/N < 20$. The error bars are our internal uncertainties. The error bar in the lower right corner of panel (b) applies to the open boxes.
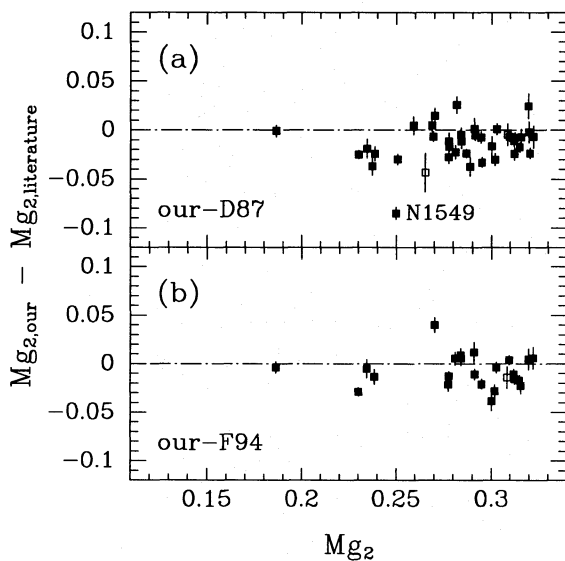
Figure 10. Comparison of our mean values with data from Davies et al. (1987) and Faber (1994, personal communication). Solid boxes – observations with $S/N \geq 20$; open boxes – observations with $S/N < 20$. The error bars are our internal uncertainties. Both the literature data and our data have been aperture-corrected with our aperture correction.

of a rectangular slit relative to the position angle of the observed galaxy was found to be within ± 0.5 per cent in the velocity dispersions. We did not correct for this effect. Our determinations of Mg_2 were offset with 0.011 to reach consistency with the Lick system, and corrected to zero velocity dispersions. From comparison with literature data we find that the typical uncertainties on the derived parameters are as follows: $\log \sigma, \pm 0.036$; $Mg_2, \pm 0.013$; $cz_{hel}, \pm 35 \text{ km s}^{-1}$.

Literature data ($\log \sigma$ and Mg_2) for galaxies in A194, DC2354$-$28 and the Coma cluster have been aperture-corrected and corrected to the same consistent system. We find that, even for aperture-corrected measurements of $\log \sigma$, offsets of 0.01–0.03 exist and should be applied in order to ensure consistency. The uncertainty of the offsets and therefore the final consistency is typically 0.01 on $\log \sigma$. The offsets may originate from the acquisition of the template stars.

The data presented here and the data from Lucey & Carter (1988) show that the use of a fibre spectrograph is highly feasible for the collection of velocity dispersions. The efficiency in terms of number of galaxies observed per night is well known in connection with redshift surveys. The accuracy of the derived velocity dispersions is, for most of the observed galaxies, high enough to make the technique useful also for studies of the FP and the large-scale motions in the Universe.

REFERENCES

Abell G. O., Corwin H. G., Jr, Olowin R. P., 1989, ApJS, 70, 1
Bender R., Döbereiner S., Möllenhoff C., 1988, A&AS, 74, 385
Chincarini G., Rood H. J., 1977, ApJ, 214, 351
Courteau S., Faber S. M., Dressler A., Willick J., 1993, ApJ, 412, L51
Cristiani S., de Souza R., D'Odorico S., Lund G., Quintana H., 1987, A&A, 179, 108
Davies R. L., Birkinshaw M., 1988, ApJS, 68, 409
Davies R. L., Efstathiou G., Fall S. M., Illingworth G., Schechter P. L., 1983, ApJ, 266, 41
Davies R. L., Burstein D., Dressler A., Faber S.M., Lynden-Bell D., Terlevich R. J., Wegner G., 1987, ApJS, 64, 581
Davies R. L., Sadler E. M., Peletier R. F., 1993, MNRAS, 262, 650
Djorgovski S., 1985, PhD thesis, Univ. California, Berkeley
Djorgovski S., Davis M., 1987, ApJ, 313, 59
Dressler A., 1980, ApJS, 42, 565
Dressler A., 1984, ApJ, 281, 512
Dressler A., 1987, ApJ, 317, 1

Dressler A., Faber S. M., Burstein D., 1991, ApJ, 368, 54

Dressler A., Faber S. M., Burstein D., Davies R. L., Lynden-Bell D., Terlevich R. J., Wegner G., 1987a, ApJ, 313, L37

Dressler A., Lynden-Bell D., Burstein D., Davies R. L., Faber S. M., Terlevich R. J., Wegner G., 1987b, ApJ, 313, 42

Dressler A., Shectman S. A., 1988, AJ, 95, 284

Faber S. M., Wegner G., Burstein D., Davies R. L., Dressler A., Lynden-Bell D., Terlevich R. J., 1989, ApJS, 69, 763

Fisher D., Illingworth G., Franx M., 1995, ApJ, 438, 539

Franx M., Illingworth G., Heckman T., 1989a, ApJ, 344, 613

Franx M., Illingworth G., Heckman T., 1989b, AJ, 98, 538

González J. J., 1993, PhD thesis, Univ. California, Santa Cruz

Guzmán R., Lucey J. R., Carter D., Terlevich R. J., 1992, MNRAS, 257, 187

Hickson P., 1982, ApJ, 255, 382

Jedrzejewski R., 1987, MNRAS, 226, 747

Jedrzejewski R., Schechter P. L., 1989, AJ, 98, 147

Jørgensen I., 1993, PhD thesis, Copenhagen University Observatory

Jørgensen I., Franx M., Kjærgaard P., 1993, ApJ, 411, 34

Jørgensen I., Franx M., Kjærgaard P., 1995a, MNRAS, 273, 1097

Jørgensen I., Franx M., Kjærgaard P., 1995b, MNRAS, submitted

Lucey J. R., Carter D., 1988, MNRAS, 235, 1177

Lucey J. R., Guzmán R., Carter D., Terlevich R. J., 1991, MNRAS, 253, 584

Lynden-Bell D., Faber S. M., Burstein D., Davies R. L., Dressler A., Terlevich R. J., Wegner G., 1988, ApJ, 326, 19

Maia M. A. G., da Costa L. N., Latham D. W., 1989, ApJS, 69, 809

Mathewson D. S., Ford V. L., Buchhorn M., 1992, ApJ, 389, L5

Peletier R. F., Davies R. L., Illingworth G. D., Davis L. E., Cawson M., 1990, AJ, 100, 1091

Phillips S., 1988, MNRAS, 233, 561

Richter O. G., 1989, A&AS, 77, 237

Richter O. G., Materne J., Huchtmeier W. K., 1982, A&A, 111, 193

Rix H.-W., White S. D. M., 1992, MNRAS, 254, 389

Sargent W. L. W., Schechter P. L., Boksenberg A., Shortridge K., 1977, ApJ, 212, 326

van der Marel R. P., Franx M., 1993, ApJ, 407, 525

van der Marel R. P., Binney J. J., Davies R. L., 1990, MNRAS, 245, 582

Whitmore B. C., McElroy D. B., Tonry J. L., 1985, ApJS, 59, 1

Willmer C. N. A., Forcardi P., Chan R., Pellegrini P. S., da Costa L. N., 1991, AJ, 101, 57

Worthey G., Faber S. M., González J. J., Burstein D., 1994, ApJS, 94, 687

APPENDIX A: OBSERVING LOG, GALAXY POSITIONS AND INDIVIDUAL MEASUREMENTS

Table A1 contains the log of the B&C observations. The positions of galaxies observed with OPTOPUS are given in Table A2. Tables A3 and A4 list the individually measured parameters from the B&C and the OPTOPUS observations, respectively.

Table A1. Log of observations.

Galaxy	Exposure time [sec]	P.A.	Obs.run	Galaxy	Exposure time [sec]	P.A.	Obs.run
A194:				**Grm15:**			
D52	3600, 3600	36*, 90*	B&C-1	A1959-56	1030	111	B&C-2
ZH07	2400	90	B&C-1	I4944	3600	170*	B&C-1
ZH09	3600	152*	B&C-1	I4952	2400	170*	B&C-1
ZH10	2400	90	B&C-1	N6848	2700	24*	B&C-1
ZH12	3600	60*	B&C-1	N6850	1800	55*	B&C-1
ZH19	3600	140*	B&C-1	N6850	1500, 1500	90*, 134	B&C-2
ZH31	3600, 3600	167*, 167*	B&C-1	N6854	3600	156	B&C-1
ZH39	3600	0	B&C-1	N6855	2400	113	B&C-1
ZH52	3600	45*	B&C-1	**HydraI − A1060:**			
ZH53	3600	145*	B&C-1	E436G44	1200	97	B&C-3
ZH56	3600	45	B&C-1	E436G45	1800	42	B&C-3
I0120	3600	40*	B&C-1	E437G21	2100	126	B&C-3
I1696	2700	5*	B&C-1	E437G45	2700	69	B&C-3
N0533	1800	130*	B&C-1	E501G03	2160	59	B&C-3
N0535	3600	90*	B&C-1	E501G13	1260	53	B&C-3
N0541	2400	90	B&C-1	I2597	2400	18	B&C-3
N0545	1800, 2100	120*, 120*	B&C-1	N3308	1260	34	B&C-3
N0547	1800, 2100	120*, 120*	B&C-1	N3309	780	47	B&C-3
N0548	3600	55*	B&C-1	N3311	2700	35	B&C-3
N0560	1800, 1800	179, 180	B&C-1	RMH28	3300	161	B&C-3
N0564	2400	54*	B&C-1	RMH72	2520	90*	B&C-3
A3381:				**Hickson groups:**			
D25	3060	40	B&C-3	H86A	2700	135*	B&C-1
D33	2700	124	B&C-3	H86B	2700	160*	B&C-1
D67	4200	46*	B&C-3	H86C	3600	90*	B&C-1
D68	4200	46*	B&C-3	H86D	3600	21*	B&C-1
D100	4200	138	B&C-3	H90B	600	90*	B&C-1
D112	4500	108	B&C-3	H90C	900	90*	B&C-1
A3574:				H90D	2700	90*	B&C-1
W22	2100	165	B&C-2	H98A	2700	40*	B&C-1
W39	3600	84	B&C-2	H98B	2700	40*	B&C-1
W47	1800	67	B&C-2	**DC2345-28:** D38	3600	135*	B&C-1
W60	2400	139	B&C-2	**Other:**			
W69	3600	13	B&C-2	A539-D16	2520	45*	B&C-3
W74	2700	17	B&C-2	E462G15	1200	90*	B&C-2
W81	2400	100	B&C-2	E553G02	1824	39	B&C-3
S639:				I2006	900, 900	125*, 125*	B&C-1
E264G24	1200	148	B&C-3	N0720	900	40*	B&C-1
E264G300	3000	84*	B&C-3	N1339	600	10*	B&C-1
E264G301	3000	84*	B&C-3	N1395	600	50*	B&C-1
J13	2400	164	B&C-3	N1399	300	90*	B&C-1
S753:				N1426	900	85*	B&C-1
W08	3600	60	B&C-2	N1439	900, 600	135*, 54	B&C-1,-3
W10	3600	90	B&C-2	N1403	600, 900	10*, 17*	B&C-1
W12	3000	77	B&C-2	N1600	1800	12	B&C-3
W17	3600	124	B&C-2	N1726	1800	5	B&C-3
W26	2400	133	B&C-2	N1794	1500	101	B&C-3
W29	1800	70*	B&C-2	N2293	600, 900	90*, 90*	B&C-2
W37	3600	8	B&C-2	N2513	900	168	B&C-3
W39	3600	118	B&C-2	N2865	900	90*	B&C-2
W47	3600	150	B&C-2	N2974	1800, 600	39	B&C-3
W49	1800	54*	B&C-2	N2986	1500, 540	30, 35	B&C-2,-3
W51	3000	146*	B&C-2	N3377	600	40	B&C-2
W54	3000	78	B&C-2	N3379	720	90*	B&C-3
W64	1200, 1200	90, 88	B&C-2	N5898	1200, 1200	180, 180	B&C-2
W73	2100	90	B&C-2	N5903	1500	166	B&C-2
W84	1500	14*	B&C-2	N6849	2400	90*	B&C-1
W95	3600	117	B&C-2	N7619	1200	90*	B&C-1
Doradus:				N7626	1200	156*	B&C-1
A0426-54	3600	135*	B&C-1				
N1411	900, 600	90*, 20	B&C-1				
N1527	900, 600	90*, 85*	B&C-1				
N1533	600	22*	B&C-1				
N1543	600, 600	85*, 90	B&C-1				
N1549	600	60*	B&C-1				
N1553	300	30*	B&C-1				
N1574	300	30*	B&C-1				
N1596	720	20	B&C-1				

References: A3574, S753 – Willmer at al. (1991). A3381, A539, DC2345−28 – Dressler (1980). A194 – Chincarini & Rood (1977), Dressler (1980). HydraI – Richter (1989). Hickson groups – Hickson (1982).

P.A. is the position angle of the slit (north through east). Except when noted with *, the slit was aligned within 5° with the major axis of the galaxy.

Table A2. OPTOPUS fields.

Galaxy	$\alpha_{1950.0}$	$\delta_{1950.0}$	field	Galaxy	$\alpha_{1950.0}$	$\delta_{1950.0}$	field
A539:				J10	10:37:44.80	-46:15:53.7	
D22	5:13:14.65	6:09:51.8		J13	10:37:49.29	-45:55:46.1	
D23	5:13:05.70	6:08:12.7		J14	10:37:51.89	-45:53:25.7	
D29	5:13:51.54	6:11:12.4		J15	10:37:52.35	-46:07:24.6	
D31	5:12:54.97	6:12:35.7		J16	10:37:53.47	-46:05:21.8	
D35	5:14:12.79	6:16:07.7		J18	10:38:02.41	-46:04:53.4	
D36	5:13:58.32	6:15:20.5		E264G301	10:38:06.46	-46:03:59.1	
D37	5:13:36.07	6:15:53.5		E264G302	10:38:09.06	-46:03:48.3	
D38	5:13:11.52	6:14:56.4		J20	10:38:15.96	-46:05:45.9	
D39	5:13:06.81	6:16:04.2		E264G31	10:38:23.37	-45:55:46.5	
D41	5:14:09.51	6:19:32.6		J23	10:38:23.38	-45:54:58.5	
D42	5:14:08.46	6:20:05.4		J26	10:38:43.00	-45:49:51.5	
D43	5:14:04.77	6:19:28.7		J31	10:39:13.59	-46:08:54.8	
D44	5:13:47.93	6:20:52.7		J32	10:39:16.23	-46:01:31.2	
D45	5:13:44.38	6:17:15.2		J101	10:38:14.92	-46:18:44.9	
D48	5:13:55.99	6:22:57.3		E264G26	10:37:33.52	-46:04:39.4	
D50	5:13:56.00	6:23:38.0		J104	10:38:54.66	-46:06:24.6	
D51	5:13:57.80	6:24:37.0		J109	10:37:33.01	-45:56:30.1	
D52	5:13:52.82	6:23:43.5		E264G28	10:37:56.24	-45:51:14.9	
D53	5:13:32.62	6:23:34.8		**Hydra:**			
D54	5:13:18.85	6:22:02.4		E501G27	10:33:36.67	-27:03:35.5	2
D57	5:14:26.12	6:26:24.2		R213	10:33:36.93	-27:18:10.9	1
D59	5:14:05.82	6:26:39.7		RMH26	10:33:43.09	-27:14:58.4	1
D60	5:14:00.36	6:26:22.8		RMH72	10:33:49.77	-27:11:41.8	1
D61	5:13:57.57	6:27:26.2		N3305	10:33:50.46	-26:54:10.6	2
D62	5:13:55.16	6:26:05.1		R219	10:33:51.90	-27:25:45.6	1
D63	5:13:54.40	6:27:01.6		R224	10:33:55.97	-27:16:13.1	1
D64	5:13:52.51	6:27:00.4		R225	10:33:57.86	-27:27:43.6	1
D68	5:14:13.80	6:29:56.5		R231	10:33:59.53	-26:54:25.6	2
D69	5:14:03.32	6:28:54.3		N3308	10:34:01.18	-27:10:44.0	1,2
D75	5:14:13.46	6:33:59.5		RMH28	10:34:01.80	-27:05:41.8	2
D76	5:14:04.89	6:34:07.2		E501G35	10:34:03.30	-26:44:23.9	2
D78	5:13:08.78	6:32:58.6		I0629	10:34:03.69	-27:19:20.4	1
A3381:				RMH29	10:34:06.36	-27:03:35.8	2
D19	6:08:34.35	-33:49:58.0		R245	10:34:07.81	-27:13:28.8	1
D20	6:07:58.05	-33:51:47.7		RMH30	10:34:10.46	-26:57:41.4	2
D21	6:07:43.97	-33:49:54.1		R253	10:34:13.72	-27:13:10.3	1
D28	6:07:32.38	-33:44:56.4		R254	10:34:14.20	-26:53:22.7	2
D33	6:09:06.04	-33:43:35.0		N3309	10:34:14.47	-27:15:31.4	1
D34	6:09:00.02	-33:43:11.4		RMH35	10:34:19.93	-27:18:05.6	1
D37	6:08:03.34	-33:40:50.2		N3311	10:34:21.50	-27:16:07.0	1
D46	6:08:32.44	-33:40:46.4		RMH79	10:34:23.64	-27:12:36.0	1
D47	6:08:11.37	-33:37:51.7		E437G11	10:34:29.46	-27:39:36.2	1
D48	6:08:05.90	-33:38:18.4		E437G13	10:34:32.89	-27:39:27.0	1
D50	6:07:40.12	-33:37:03.2		R308	10:34:48.38	-27:23:53.0	1
D55	6:08:04.50	-33:34:53.4		R303	10:34:43.55	-27:08:24.8	2
D56	6:07:59.43	-33:35:12.6		E501G47	10:34:55.72	-27:12:32.7	1,2
D64	6:08:44.42	-33:30:59.1		N3315	10:34:57.78	-26:55:56.4	2
D67	6:08:09.39	-33:32:20.9		R319	10:34:58.00	-27:00:48.9	2
D69	6:07:40.83	-33:32:33.0		E501G49	10:34:58.64	-27:17:59.0	1
D72	6:08:31.44	-33:28:56.1		R327	10:35:03.52	-27:36:51.1	1
D73	6:08:27.47	-33:26:52.6		N3316	10:35:15.97	-27:20:02.7	1
D75	6:08:21.25	-33:28:12.6		R338	10:35:18.96	-26:47:52.6	2
D76	6:08:02.51	-33:29:35.0		RMH50	10:35:19.95	-26:47:03.9	2
D91	6:08:36.53	-33:23:03.2		I2597	10:35:25.65	-26:49:18.3	2
S639:							
E264G23	10:36:59.41	-46:14:40.9					
E264G24	10:37:01.87	-45:52:49.6					
J06	10:37:30.69	-46:01:50.8					
J09	10:37:37.00	-45:52:59.9					

References: A3381 and A539 – Dressler (1980). HydraI – Richter et al. (1982) and Richter (1989).

Table A3. Spectroscopic parameters for B&C spectra.

Galaxy	cz_{hel}	$\log \sigma$ (obs)	$\log \sigma$ (3″4)	$\sigma_{\log \sigma}$	Mg_2 (obs)	Mg_2 (3″4)	σ_{Mg_2}	S/N	B&C run
A194:									
D52	6319	1.883	1.884	0.054	0.178	0.179	0.014	14.6	1
D52	6291	1.866	1.866	0.063	0.218	0.219	0.017	12.1	1
I0120	4806	2.039	2.040	0.053	0.235	0.235	0.017	12.6	1
I1696	5827	2.185	2.186	0.022	0.284	0.284	0.007	29.2	1
N0533	5606	2.411	2.412	0.032	0.308	0.308	0.011	19.3	1
N0535	4906	2.110	2.111	0.046	0.229	0.230	0.015	14.1	1
N0541	5453	2.282	2.283	0.030	0.288	0.289	0.009	22.5	1
N0545	5312	2.376	2.376	0.020	0.301	0.301	0.007	30.1	1
N0545	5347	2.353	2.353	0.019	0.289	0.289	0.007	31.4	1
N0547	5534	2.376	2.376	0.018	0.307	0.308	0.006	34.6	1
N0547	5561	2.413	2.413	0.019	0.311	0.312	0.007	31.0	1
N0548	5410	2.092	2.092	0.035	0.234	0.235	0.010	21.9	1
N0560	5491	2.252	2.253	0.023	0.271	0.271	0.008	25.3	1
N0560	5525	2.255	2.256	0.020	0.269	0.269	0.007	29.2	1
N0564	5836	2.355	2.355	0.022	0.281	0.281	0.007	31.8	1
ZH07	5785	2.180	2.181	0.026	0.242	0.242	0.009	24.2	1
ZH09	5535	2.085	2.085	0.026	0.232	0.232	0.008	27.8	1
ZH10	5296	2.320	2.321	0.027	0.302	0.303	0.010	21.6	1
ZH12	5237	2.211	2.211	0.019	0.246	0.246	0.007	32.0	1
ZH19	4489	2.052	2.052	0.025	0.221	0.222	0.007	28.5	1
ZH31	5929	1.835	1.835	0.048	0.171	0.172	0.011	18.6	1
ZH31	5953	1.829	1.830	0.060	0.200	0.201	0.015	13.7	1
ZH39	4853	2.279	2.280	0.019	0.257	0.257	0.006	35.2	1
ZH52	5592	2.011	2.011	0.043	0.285	0.286	0.010	21.0	1
ZH53	5712	1.934	1.934	0.039	0.189	0.190	0.010	19.7	1
ZH56	8269	2.328	2.328	0.018	0.294	0.295	0.006	35.4	1
A3381:									
D25	11495	2.293	2.306	0.023	0.262	0.275	0.009	22.7	3
D33	11707	2.306	2.319	0.022	0.209	0.222	0.008	25.5	3
D68	11335	2.181	2.194	0.037	0.258	0.271	0.014	14.6	3
D100	11488	2.297	2.310	0.028	0.258	0.271	0.011	19.9	3
D112	11059	2.334	2.347	0.029	0.262	0.275	0.011	19.9	3
A3574:									
W22	4585	2.330	2.330	0.017	0.295	0.295	0.006	34.2	2
W39	5095	2.166	2.166	0.021	0.247	0.247	0.008	26.6	2
W47	4560	2.392	2.392	0.018	0.312	0.312	0.006	33.6	2
W60	3763	2.349	2.349	0.022	0.248	0.248	0.007	29.1	2
W69	5405	1.935	1.935	0.026	0.158	0.158	0.006	32.6	2
W74	4251	2.320	2.320	0.017	0.286	0.286	0.007	32.4	2
W81	4571	2.271	2.271	0.019	0.276	0.277	0.007	30.2	2
S639:									
E264G24	6031	2.336	2.339	0.021	0.257	0.261	0.009	22.4	3
E264G300	6140	2.445	2.449	0.023	0.297	0.301	0.008	27.3	3
E264G301	5329	2.178	2.182	0.035	0.264	0.267	0.011	18.6	3
J13	6574	2.309	2.313	0.023	0.251	0.255	0.009	22.4	3
S753:									
W08	3966	2.056	2.055	0.020	0.224	0.222	0.008	27.7	2
W10	3962	2.102	2.100	0.017	0.216	0.215	0.006	35.8	2
W12	4169	2.203	2.201	0.018	0.271	0.270	0.007	28.6	2
W17	4175	1.995	1.993	0.026	0.187	0.185	0.008	26.1	2
W26	3449	2.155	2.154	0.018	0.235	0.233	0.007	30.2	2
W29	4161	2.422	2.420	0.024	0.294	0.292	0.008	28.0	2
W37	3924	2.224	2.222	0.020	0.288	0.286	0.006	34.3	2
W39	10630	2.333	2.332	0.028	0.269	0.268	0.009	23.8	2
W47	4266	2.069	2.067	0.031	0.239	0.237	0.010	20.3	2
W49	5135	2.388	2.387	0.019	0.290	0.288	0.006	34.2	2
W51	4026	2.173	2.171	0.024	0.236	0.235	0.009	22.4	2
W54	4697	2.250	2.248	0.018	0.249	0.247	0.006	34.2	2
W64	4187	2.500	2.498	0.023	0.320	0.318	0.007	29.3	2
W64	4202	2.550	2.548	0.024	0.324	0.322	0.008	28.6	2
W73	3849	2.262	2.260	0.019	0.290	0.289	0.007	30.6	2
W84	4498	2.320	2.318	0.024	0.283	0.282	0.009	24.8	2
W95	4659	2.110	2.108	0.020	0.249	0.247	0.007	29.1	2
Doradus:									
A0426-54	1547	1.678	1.653	0.102	0.099	0.075	0.009	21.0	1
N1411	1036	2.090	2.065	0.019	0.228	0.203	0.005	38.3	1
N1411	1005	2.152	2.127	0.017	0.224	0.199	0.005	41.6	1
N1527	1210	2.241	2.216	0.017	0.272	0.248	0.006	34.6	1
N1527	1187	2.202	2.177	0.018	0.272	0.248	0.006	33.3	1
N1533	821	2.267	2.243	0.024	0.294	0.270	0.009	23.1	1
N1543	1198	2.167	2.142	0.018	0.295	0.270	0.007	31.8	1
N1543	1211	2.212	2.188	0.025	0.281	0.256	0.009	23.1	1
N1549	1259	2.317	2.293	0.018	0.275	0.250	0.006	34.4	1
N1553	1247	2.239	2.215	0.020	0.276	0.252	0.007	28.5	1
N1574	1030	2.338	2.313	0.020	0.298	0.274	0.008	27.3	1

Table A3 – *continued*

Galaxy	cz_{hel}	$\log\sigma$ (obs)	$\log\sigma$ (3″.4)	$\sigma_{\log\sigma}$	Mg_2 (obs)	Mg_2 (3″.4)	σ_{Mg_2}	S/N	B&C run
N1596	1534	2.221	2.196	0.016	0.283	0.259	0.005	40.0	1
Grm15:									
A1959-56	4464	2.420	2.419	0.024	0.320	0.319	0.009	24.8	2
I4944	5890	2.082	2.080	0.041	0.148	0.147	0.008	25.3	1
I4952	4289	2.124	2.123	0.030	0.214	0.213	0.008	27.3	1
N6848	4447	2.257	2.256	0.021	0.229	0.227	0.008	27.1	1
N6850	4920	2.262	2.261	0.019	0.218	0.217	0.006	32.9	1
N6850	4891	2.181	2.180	0.027	0.215	0.214	0.010	21.8	2
N6850	4893	2.293	2.292	0.027	0.199	0.198	0.010	20.9	2
N6854	5747	2.329	2.328	0.019	0.289	0.288	0.005	40.0	1
N6855	4426	2.283	2.282	0.040	0.308	0.307	0.007	31.4	1
HydraI – A1060:									
E436G44	3165	2.218	2.213	0.024	0.250	0.246	0.009	22.4	3
E436G45	3402	2.283	2.279	0.028	0.259	0.255	0.010	22.2	3
E437G21	3931	2.253	2.248	0.019	0.275	0.271	0.008	26.5	3
E437G45	3757	2.107	2.103	0.031	0.271	0.267	0.014	15.5	3
E501G03	4199	2.327	2.323	0.018	0.276	0.272	0.008	26.8	3
E501G13	3520	2.356	2.352	0.021	0.297	0.293	0.009	24.2	3
I2597	3011	2.431	2.427	0.018	0.308	0.304	0.007	31.7	3
N3308	3581	2.268	2.263	0.024	0.295	0.291	0.011	20.3	3
N3309	4113	2.467	2.463	0.024	0.326	0.322	0.011	19.3	3
N3311	3875	2.285	2.280	0.030	0.324	0.320	0.012	17.5	3
RMH28	3025	2.169	2.165	0.026	0.265	0.261	0.011	18.6	3
RMH72	4923	2.080	2.076	0.025	0.242	0.238	0.010	21.9	3
Hickson groups:									
H86A	6062	2.396	2.398	0.024	0.320	0.323	0.008	27.1	1
H86B	5837	2.310	2.313	0.026	0.272	0.275	0.008	26.8	1
H86C	5317	2.237	2.239	0.036	0.292	0.294	0.015	14.6	1
H86D	6019	2.272	2.274	0.025	0.271	0.274	0.007	31.0	1
H90B	2551	2.422	2.410	0.023	0.317	0.305	0.009	24.8	1
H90C	2600	2.278	2.266	0.019	0.285	0.273	0.007	31.0	1
H90D	2711	2.144	2.132	0.032	0.185	0.173	0.009	23.1	1
H98A	7947	2.389	2.396	0.020	0.269	0.276	0.007	29.4	1
H98B	7999	2.383	2.390	0.023	0.284	0.291	0.008	27.6	1
DC2345-28:									
D38	9049	2.056	2.070	0.054	0.270	0.284	0.017	12.6	1
Other:									
A539-D16	9695	2.286	2.295	0.030	0.268	0.276	0.010	20.3	3
E462G15	5844	2.457	2.459	0.026	0.275	0.277	0.009	24.3	2
E553G02	4814	2.407	2.406	0.060	0.267	0.265	0.020	10.8	3
I2006	1394	2.103	2.081	0.019	0.277	0.255	0.007	29.7	1
I2006	1382	2.077	2.055	0.023	0.267	0.245	0.008	25.8	1
N0720	1722	2.381	2.361	0.015	0.333	0.312	0.005	41.6	1
N1339	1332	2.227	2.205	0.019	0.306	0.284	0.007	31.2	1
N1395	1698	2.395	2.375	0.018	0.323	0.303	0.006	38.3	1
N1399	1454	2.557	2.535	0.022	0.337	0.316	0.008	26.8	1
N1403	4286	2.192	2.189	0.033	0.267	0.264	0.012	17.1	1
N1403	4278	2.214	2.211	0.036	0.211	0.208	0.013	15.9	1
N1426	1422	2.190	2.170	0.020	0.259	0.239	0.007	28.8	1
N1439	1681	2.103	2.083	0.029	0.289	0.269	0.010	20.7	1
N1439	1678	2.167	2.146	0.025	0.293	0.272	0.011	18.6	3
N1600	4760	2.473	2.472	0.030	0.321	0.320	0.011	20.3	3
N1726	3989	2.391	2.387	0.016	0.282	0.278	0.007	32.6	3
N1794	5002	2.271	2.270	0.030	0.207	0.206	0.008	24.7	3
N2293	2014	2.406	2.392	0.025	0.312	0.299	0.010	21.8	2
N2293	2031	2.413	2.400	0.018	0.306	0.292	0.007	30.8	2
N2513	4728	2.470	2.469	0.026	0.301	0.300	0.010	21.5	3
N2865	2651	2.225	2.216	0.018	0.195	0.186	0.006	35.8	2
N2974	1925	2.421	2.408	0.016	0.287	0.274	0.006	36.4	3
N2974	1915	2.423	2.409	0.020	0.298	0.284	0.007	28.7	3
N2986	2314	2.404	2.393	0.023	0.330	0.318	0.009	23.3	3
N2986	2323	2.382	2.371	0.020	0.319	0.309	0.007	31.8	2
N3377	716	2.156	2.132	0.013	0.254	0.230	0.004	48.0	2
N3379	912	2.325	2.300	0.015	0.316	0.291	0.005	41.5	3
N5898	2165	2.384	2.373	0.018	0.302	0.291	0.006	35.8	2
N5898	2151	2.364	2.353	0.016	0.293	0.282	0.006	35.8	2
N5903	2556	2.303	2.292	0.016	0.280	0.269	0.006	33.2	2
N6849	6100	2.298	2.301	0.026	0.256	0.259	0.009	22.8	1
N7619	3793	2.479	2.472	0.016	0.322	0.315	0.005	43.2	1
N7626	3405	2.430	2.423	0.017	0.309	0.302	0.006	35.0	1

Notes. cz_{hel} – the heliocentric radial velocity; the internal uncertainty is typically 17 km s^{-1}. $\sigma_{\log\sigma}$ – the formal uncertainty on $\log\sigma$ as derived from the fit. (obs) – raw measurements. (3″.4) – aperture corrected to $2r_{norm} = 1.19$ h^{-1} kpc, equivalent to 3.4 arcsec at the distance of the Coma cluster.

Table A4. Spectroscopic parameters for OPTOPUS spectra.

| Galaxy | Observation 1 | | | | Observation 2 | | | | Mean values | | | | | | | |
	cz_{hel}	$\log\sigma$	Mg_2	S/N	cz_{hel}	$\log\sigma$	Mg_2	S/N	cz_{hel}	$\log\sigma$ (obs)	$\log\sigma$ (3″.4)	$\sigma_{\log\sigma}$	Mg_2 (obs)	Mg_2 (3″.4)	σ_{Mg_2}	S/N
A539:																
D22	⋯	⋯	⋯	⋯	⋯	⋯	⋯	⋯	13041	2.111	2.110	0.034	0.183	0.182	0.008	25.6
D23	⋯	⋯	⋯	⋯	⋯	⋯	⋯	⋯	12242	2.051	2.050	0.064	0.200	0.199	0.014	15.0
D29	⋯	⋯	⋯	⋯	⋯	⋯	⋯	⋯	8529	2.095	2.094	0.040	0.241	0.240	0.009	22.6
D31	8737	2.204	0.229	23.4	8746	2.146	0.233	24.4	8742	2.178	2.176	0.021	0.231	0.230	0.006	⋯
D35	8075	2.272	0.282	22.3	8054	2.250	0.274	22.3	8063	2.261	2.260	0.022	0.278	0.277	0.007	⋯
D36	⋯	⋯	⋯	⋯	⋯	⋯	⋯	⋯	8382	2.064	2.063	0.031	0.267	0.266	0.009	24.0
D37	9834	2.231	0.271	27.7	9845	2.224	0.274	26.4	9838	2.228	2.227	0.017	0.272	0.271	0.006	⋯
D38	9203	2.184	0.257	22.8	9212	2.234	0.259	22.3	9209	2.216	2.214	0.022	0.258	0.257	0.007	⋯
D39	8633	2.182	0.257	27.7	8635	2.221	0.247	28.2	8634	2.204	2.202	0.018	0.252	0.251	0.005	⋯
D41	8114	2.198	0.248	22.8	8147	2.151	0.255	21.1	8129	2.180	2.179	0.025	0.251	0.250	0.007	⋯
D42	8675	2.136	0.257	22.3	8680	2.168	0.252	21.7	8677	2.153	2.152	0.022	0.254	0.253	0.007	⋯
D43	⋯	⋯	⋯	⋯	⋯	⋯	⋯	⋯	8410	2.068	2.067	0.029	0.188	0.187	0.008	24.8
D44	7419	2.260	0.258	32.7	7440	2.290	0.264	34.5	7429	2.275	2.274	0.013	0.261	0.260	0.004	⋯
D45	8699	2.312	0.305	32.3	8722	2.352	0.304	30.7	8708	2.331	2.330	0.015	0.305	0.303	0.005	⋯
D48	7732	2.251	0.301	26.8	7752	2.240	0.268	25.9	7741	2.246	2.245	0.019	0.285	0.284	0.005	⋯
D50	8674	2.349	0.296	29.0	8677	2.311	0.264	27.3	8675	2.333	2.331	0.017	0.281	0.279	0.005	⋯
D51	9362	2.196	0.246	26.8	9364	2.200	0.258	26.4	9363	2.198	2.197	0.018	0.252	0.251	0.006	⋯
D52	⋯	⋯	⋯	⋯	⋯	⋯	⋯	⋯	8079	2.122	2.121	0.030	0.258	0.257	0.008	26.8
D53	6667	2.390	0.287	28.2	6662	2.328	0.239	27.7	6664	2.362	2.360	0.016	0.263	0.262	0.005	⋯
D54	⋯	⋯	⋯	⋯	⋯	⋯	⋯	⋯	8838	2.115	2.114	0.024	0.244	0.243	0.007	29.0
D57	10030	2.259	0.297	23.9	9993	2.162	0.282	21.7	10012	2.225	2.223	0.024	0.290	0.289	0.007	⋯
D59	7206	2.157	0.265	23.9	7218	2.258	0.271	22.3	7210	2.209	2.208	0.023	0.268	0.267	0.006	⋯
D60	9752	2.374	0.257	27.3	9754	2.397	0.255	25.9	9753	2.385	2.384	0.018	0.256	0.255	0.006	⋯
D61	7884	2.117	0.265	22.3	7872	2.150	0.251	20.5	7879	2.134	2.132	0.023	0.258	0.257	0.007	⋯
D62	9281	2.264	0.272	26.8	9299	2.244	0.266	25.4	9292	2.253	2.252	0.019	0.269	0.268	0.006	⋯
D63	7106	2.228	0.231	38.6	7095	2.250	0.218	37.3	7101	2.238	2.237	0.015	0.225	0.223	0.004	⋯
D64	8667	2.143	0.228	23.9	8677	2.152	0.209	22.3	8672	2.147	2.146	0.021	0.219	0.218	0.006	⋯
D68	9700	2.508	0.327	42.6	9699	2.471	0.322	40.5	9699	2.490	2.488	0.013	0.325	0.324	0.004	⋯
D69	9924	2.386	0.299	24.9	9938	2.312	0.284	22.3	9931	2.356	2.355	0.021	0.292	0.291	0.006	⋯
D75	⋯	⋯	⋯	⋯	⋯	⋯	⋯	⋯	9100	2.094	2.093	0.026	0.271	0.270	0.008	27.9
D76	⋯	⋯	⋯	⋯	⋯	⋯	⋯	⋯	7962	2.138	2.136	0.042	0.196	0.195	0.010	21.2
D78	⋯	⋯	⋯	⋯	⋯	⋯	⋯	⋯	9361	2.209	2.207	0.025	0.248	0.247	0.008	27.5
A3381:																
D19	⋯	⋯	⋯	⋯	⋯	⋯	⋯	⋯	12048	1.870	1.873	0.082	0.147	0.151	0.014	14.3
D20	⋯	⋯	⋯	⋯	⋯	⋯	⋯	⋯	11523	1.953	1.956	0.041	0.170	0.173	0.008	25.2
D21	11311	2.273	0.287	32.6	11310	2.258	0.287	30.0	11311	2.266	2.270	0.017	0.287	0.290	0.005	⋯
D28	10975	2.087	0.249	24.0	10938	2.137	0.227	23.4	10954	2.119	2.122	0.024	0.238	0.242	0.006	⋯
D33	⋯	⋯	⋯	⋯	⋯	⋯	⋯	⋯	11667	2.182	2.186	0.037	0.226	0.230	0.011	18.7
D34	⋯	⋯	⋯	⋯	⋯	⋯	⋯	⋯	11355	2.349	2.352	0.034	0.228	0.231	0.010	20.2
D37	⋯	⋯	⋯	⋯	⋯	⋯	⋯	⋯	11154	1.954	1.957	0.058	0.195	0.198	0.011	18.1
D46	⋯	⋯	⋯	⋯	⋯	⋯	⋯	⋯	8981	2.041	2.044	0.049	0.203	0.206	0.010	20.7
D47	⋯	⋯	⋯	⋯	⋯	⋯	⋯	⋯	8755	1.881	1.885	0.050	0.141	0.144	0.007	29.0
D48	8899	2.202	0.230	30.9	8902	2.025	0.238	25.6	8900	2.152	2.156	0.020	0.233	0.236	0.005	⋯
D50	⋯	⋯	⋯	⋯	⋯	⋯	⋯	⋯	11226	2.084	2.087	0.041	0.233	0.236	0.008	24.8
D55	11561	2.312	0.314	28.6	11549	2.302	0.294	22.8	11557	2.309	2.312	0.018	0.306	0.309	0.006	⋯
D56	⋯	⋯	⋯	⋯	⋯	⋯	⋯	⋯	11306	2.315	2.318	0.030	0.293	0.296	0.009	23.5
D64	⋯	⋯	⋯	⋯	⋯	⋯	⋯	⋯	11487	2.110	2.114	0.061	0.172	0.175	0.014	14.3
D67	⋯	⋯	⋯	⋯	⋯	⋯	⋯	⋯	11255	2.035	2.039	0.058	0.236	0.239	0.013	15.7
D69	⋯	⋯	⋯	⋯	⋯	⋯	⋯	⋯	10375	2.033	2.036	0.074	0.181	0.184	0.014	15.0
D72	⋯	⋯	⋯	⋯	⋯	⋯	⋯	⋯	10956	1.829	1.832	0.108	0.161	0.164	0.016	12.9
D73	⋯	⋯	⋯	⋯	⋯	⋯	⋯	⋯	11213	2.097	2.101	0.084	0.228	0.231	0.020	10.4
D75	⋯	⋯	⋯	⋯	⋯	⋯	⋯	⋯	11463	2.312	2.315	0.026	0.253	0.256	0.008	27.5
D76	⋯	⋯	⋯	⋯	⋯	⋯	⋯	⋯	15106	2.258	2.261	0.046	⋯	⋯	⋯	19.2
D91	⋯	⋯	⋯	⋯	⋯	⋯	⋯	⋯	9178	1.932	1.935	0.089	0.210	0.214	0.018	11.4
S639:																
E264G23	5678	2.313	⋯	32.6	5629	2.337	⋯	23.5	5658	2.324	2.318	0.018	⋯	⋯	⋯	⋯
E264G24	6128	2.344	0.269	46.6	6104	2.316	0.260	37.1	6118	2.333	2.327	0.011	0.266	0.260	0.004	⋯
E264G26	⋯	⋯	⋯	⋯	⋯	⋯	⋯	⋯	6339	2.097	2.091	0.025	0.237	0.231	0.007	31.0
E264G28	6606	2.164	0.236	32.3	6595	2.190	0.236	21.6	6603	2.173	2.167	0.017	0.236	0.230	0.005	⋯
E264G301	5363	2.267	⋯	35.9	5380	2.262	⋯	23.1	5369	2.265	2.259	0.016	⋯	⋯	⋯	⋯
E264G302	⋯	⋯	⋯	⋯	⋯	⋯	⋯	⋯	6482	2.258	2.252	0.022	0.255	0.249	0.006	33.0
E264G31	6697	2.380	0.287	32.6	6692	2.367	0.262	29.4	6694	2.374	2.368	0.014	0.275	0.269	0.005	⋯
J06	⋯	⋯	⋯	⋯	⋯	⋯	⋯	⋯	6470	2.023	2.017	0.040	0.195	0.189	0.009	23.1
J09	⋯	⋯	⋯	⋯	⋯	⋯	⋯	⋯	6253	1.834	1.828	0.105	0.204	0.198	0.018	11.3
J10	⋯	⋯	⋯	⋯	⋯	⋯	⋯	⋯	6814	1.838	1.832	0.061	0.186	0.180	0.011	18.1
J13	6650	2.291	0.261	38.8	6644	2.249	0.243	27.9	6647	2.273	2.267	0.015	0.255	0.249	0.004	⋯
J14	⋯	⋯	⋯	⋯	⋯	⋯	⋯	⋯	5682	2.117	2.111	0.023	⋯	⋯	⋯	31.4
J15	5867	2.073	⋯	28.6	5839	2.100	⋯	25.4	5854	2.087	2.081	0.020	⋯	⋯	⋯	⋯
J16	⋯	⋯	⋯	⋯	⋯	⋯	⋯	⋯	5925	2.076	2.070	0.027	⋯	⋯	⋯	25.6
J18	⋯	⋯	⋯	⋯	⋯	⋯	⋯	⋯	5959	1.917	1.911	0.077	⋯	⋯	⋯	10.9
J20	⋯	⋯	⋯	⋯	⋯	⋯	⋯	⋯	5546	1.615	1.609	0.134	⋯	⋯	⋯	14.3
J23	⋯	⋯	⋯	⋯	⋯	⋯	⋯	⋯	6367	2.122	2.116	0.034	0.243	0.237	0.009	24.0
J26	⋯	⋯	⋯	⋯	⋯	⋯	⋯	⋯	6663	2.478	2.472	0.019	0.295	0.289	0.006	38.1

Table A4 – *continued*

| Galaxy | Observation 1 | | | | Observation 2 | | | | Mean values | | | | | | | |
	cz_{hel}	$\log\sigma$	Mg_2	S/N	cz_{hel}	$\log\sigma$	Mg_2	S/N	cz_{hel}	$\log\sigma$ (obs)	$\log\sigma$ (3".4)	$\sigma_{\log\sigma}$	Mg_2 (obs)	Mg_2 (3".4)	σ_{Mg_2}	S/N
J31	...	...	...	...	...	...	...	...	5805	1.697	1.691	0.159	...	...	...	13.2
J32	6551	2.192	0.266	31.2	6516	2.122	0.252	23.1	6536	2.169	2.163	0.017	0.261	0.255	0.005	...
J101	...	...	...	...	...	...	...	...	7085	1.942	1.936	0.042	0.204	0.198	0.010	21.2
J104	...	...	...	...	...	...	...	...	6547	2.000	1.994	0.068	0.131	0.125	0.010	20.7
J109	...	...	...	...	...	...	...	...	6956	2.136	2.130	0.019	0.246	0.240	0.006	34.8
HydraI: – A1060																
E437G11	4944	2.296	...	35.9	4932	2.220	...	27.2	4938	2.265	2.251	0.015	...	...	...	...
E437G13	3504	2.218	...	51.6	3493	2.208	...	35.4	3499	2.214	2.200	0.012	...	...	...	...
E501G27	...	...	...	...	...	...	...	...	3230	1.728	1.715	0.072	...	...	...	22.2
E501G35	4185	2.176	...	53.6	4177	2.144	...	49.6	4181	2.162	2.148	0.010	...	...	...	...
E501G47	4790	2.160	...	26.8	4841	2.132	...	22.6	...	...	...	...	...	...	...	...
E501G47	4874	2.074	...	29.3	...	...	...	...	4838	2.125	2.111	0.015	...	...	...	...
E501G49	...	...	...	...	...	...	...	...	4063	2.026	2.012	0.022	...	...	...	33.0
I0629	2820	2.065	...	29.7	2827	1.993	...	22.2	2822	2.047	2.034	0.020	...	...	...	...
I2597	2935	2.319	...	29.0	2955	2.358	...	30.0	2946	2.343	2.329	0.018	...	...	...	...
N3305	3982	2.385	...	65.6	3971	2.378	...	64.0	3976	2.381	2.367	0.010	...	...	...	...
N3308	3575	2.286	...	28.3	3574	2.272	...	29.7	...	...	...	...	...	...	...	...
N3308	3541	2.265	...	29.0	3568	2.302	...	27.5	3564	2.284	2.270	0.012	...	...	...	...
N3309	4086	2.395	...	60.7	4096	2.404	...	55.4	4091	2.400	2.386	0.010	...	...	...	...
N3311	3878	2.277	...	26.8	3851	2.292	...	24.8	3865	2.284	2.270	0.018	...	...	...	...
N3315	3789	2.201	...	33.9	3800	2.202	...	37.9	3793	2.201	2.187	0.015	...	...	...	...
N3316	3878	2.232	...	49.6	3873	2.194	...	37.1	3876	2.218	2.204	0.012	...	...	...	...
R213	3580	1.999	...	31.7	3587	1.965	...	25.2	3583	1.987	1.973	0.017	...	...	...	...
R219	...	...	...	...	...	...	...	...	4188	2.013	1.999	0.022	...	...	...	33.9
R224	...	...	...	...	...	...	...	...	3764	2.003	1.989	0.033	...	...	...	31.0
R225	...	...	...	...	...	...	...	...	3522	1.927	1.913	0.031	...	...	...	27.5
R231	...	...	...	...	...	...	...	...	3685	1.932	1.918	0.031	...	...	...	29.7
R245	4795	2.035	...	28.3	4781	2.083	...	21.2	4789	2.058	2.044	0.020	...	...	...	...
R253	...	...	...	...	...	...	...	...	4686	1.894	1.880	0.034	...	...	...	26.8
R254	...	...	...	...	...	...	...	...	4662	1.651	1.637	0.098	...	...	...	19.2
R261	...	...	...	...	...	...	...	...	3807	1.806	1.792	0.079	...	...	...	18.7
R293	...	...	...	...	...	...	...	...	4482	1.633	1.619	0.124	...	...	...	13.4
R303	...	...	...	...	...	...	...	...	2758	1.957	1.943	0.037	...	...	...	29.7
R308	...	...	...	...	...	...	...	...	4103	2.076	2.062	0.027	...	...	...	33.3
R319	...	...	...	...	...	...	...	...	4460	1.855	1.841	0.050	...	...	...	23.1
R327	...	...	...	...	...	...	...	...	4213	1.956	1.942	0.045	...	...	...	21.7
R338	...	...	...	...	...	...	...	...	4372	1.740	1.726	0.074	...	...	...	20.7
RMH26	2292	2.024	...	29.3	2280	2.001	...	25.6	2286	2.014	2.000	0.019	...	...	...	...
RMH28	...	...	...	...	...	...	...	...	2982	2.110	2.096	0.033	...	...	...	24.4
RMH29	3431	2.164	...	26.4	3452	2.182	...	30.4	3441	2.174	2.160	0.018	...	...	...	...
RMH30	10670	2.253	0.271	21.7	10673	2.293	0.276	21.7	10672	2.275	2.262	0.021	0.273	0.259	0.007	...
RMH35	4737	2.064	...	41.2	4745	2.107	...	26.0	4739	2.080	2.066	0.015	...	...	...	...
RMH50	3072	1.877	...	27.2	3078	1.998	...	30.4	3075	1.953	1.939	0.022	...	...	...	...
RMH72	4870	2.062	...	35.1	4909	2.073	...	27.9	4884	2.066	2.052	0.016	...	...	...	...
RMH79	2712	2.304	...	47.5	2663	2.171	...	35.4	2687	2.258	2.244	0.015	...	...	...	...

Notes. cz_{hel} – the heliocentric radial velocity; the internal uncertainty is typically 17 km s^{-1}. $\sigma_{\log\sigma}$ – the formal uncertainty on $\log\sigma$, as derived from the fit; the mean values are weighted with the variance (for galaxies where individual measurements are not given, the parameters were derived from the mean spectra). (obs) – mean of the raw measurements. (3".4) – aperture-corrected to $2r_{norm} = 1.19\ h^{-1}$ kpc, equivalent to 3.4 arcsec at the distance of the Coma cluster.